PHYSICAL REVIEW B VOLUME 43, NUMBER 7 1 MARCH 1991

Polarization and resonance studies of x-ray magnetic scattering in holmium

Doon Gibbs and G. Grübel
Physics Department, Brookhaven National Laboratory, Upton, New York 11973

D. R. Harshman, E. D. Isaacs, and D. B. McWhan*
AT&T Bell Laboratories, 600 Mountain Ave., Murray Hill, New Jersey 07973

D. Mills†
CHESS, Cornell University, Ithaca, New York 14853

C. Vettier‡
Institut Laue-Langevin, 38042, Grenoble, CEDEX, France

(Received 25 July 1990)

We report the results of an x-ray-scattering study of the polarization and resonance properties of the magnetic cross section of holmium. Off resonance, we have measured the degree of linear polarization for several different chemical and magnetic reflections, and shown that the results are consistent with a nonresonant description of the x-ray-scattering cross section. When the incident x-ray energy is tuned near the L_{III} absorption edge, large resonant enhancements of the magnetic scattering, and resonant integer harmonics, are observed. Detailed measurements of the dependence of the integrated magnetic intensity on the incident x-ray energy, on the x-ray momentum transfer, and on the sample temperature are described for incident x-ray energies in a range of 250 eV below and above the L_{III} absorption edge. In addition, we have characterized the energy dependence of the linearly σ- and π-polarized components of the magnetic scattering in this range, and fitted the resulting line shapes to a simple model of the resonant cross section, including electric dipole and quadrupole transitions among atomic orbitals. The most striking feature of the line shapes is their asymmetry, which results from the interference of the resonant and nonresonant cross sections. Smaller resonant enhancements of the magnetic scattering are reported for incident x-ray energies tuned near the L_{II} and L_{I} absorption edges.

I. INTRODUCTION

In this paper, we present the results of an x-ray-scattering study of the rare-earth metal holmium. Our main purpose in this work has been to explore basic elements of the polarization and resonance properties of the x-ray magnetic cross section. Specifically, for linearly σ-polarized incident x radiation, we have examined the dependence of the integrated magnetic intensity on the incident x-ray energy, on the x-ray momentum transfer, and on the sample temperature, as the incident x-ray energy is tuned near to and far from the L_{III}, L_{II}, and L_{I} absorption edges. In addition, we have characterized the energy dependence of the linearly σ- and π-polarized components of the scattered x-ray beam, and fitted the resulting line shapes to a simple model of the resonant x-ray cross section.[1-3] The experiments described in this paper were motivated, in part, by earlier experiments on holmium[1,2] in which attempts were made to distinguish the contributions of the orbital- and spin-magnetization densities to the magnetic cross section by analyzing the polarization of the scattered beam. In addition, an approximately fiftyfold resonant enhancement of the x-ray magnetic scattering, and resonant integer harmonics, were discovered when the incident x-ray energy was tuned near the L_{III} absorption edge.[1,2] Besides intrinsic interest in the x-ray-scattering cross section and its description, studies of this type are also motivated by the possibility that new structural and magnetic properties of rare-earth metals might be revealed, and that new techniques may thereby be developed. In this regard, the spiral antiferromagnetic holmium offers a unique opportunity for detailed analysis. By virtue of its large magnetic moment and incommensurate magnetic structure, x-ray magnetic scattering is readily detected using synchrotron radiation. Further, the detailed magnetic structure of holmium is well established on the basis of a variety of earlier x-ray- and neutron-scattering studies.[4-12]

The results described in this paper are analyzed within two regimes of the incident x-ray energy, namely, in the limit of high-x-ray energies, when the incident x-ray energy lies above the excitation energy of any absorption edge, and at resonance, when the incident energy lies near an absorption edge. In the high-energy limit, the amplitude for x-ray magnetic scattering has the simple form $[\mathbf{L}(\mathbf{Q})\cdot\mathbf{A}+\mathbf{S}(\mathbf{Q})\cdot\mathbf{B}]$.[13-15] Here, $\mathbf{L}(\mathbf{Q})$ and $\mathbf{S}(\mathbf{Q})$ refer to the Fourier transforms of the atomic orbital- and spin-magnetization densities, respectively, and the vectors $\mathbf{A}$ and $\mathbf{B}$ depend on the incident and scattered wave vectors and on the incident and scattered polarization vectors.[13-15] Because the vectors $\mathbf{A}$ and $\mathbf{B}$ are not identical, the polarization dependence of the orbital contribution to the magnetic cross section differs from that of the spin contribution. This leads to the possibility that the orbital- and spin-magnetization densities may be distinguished in x-ray-scattering experiments. The same distinction is not directly possible by neutron-diffraction techniques (in dipole approximation, where the polarization dependence of the orbital contribution is identical to that of the spin contribution), and is important to a fundamental understanding of the electronic structure of magnetic materials. A particular class of experiments for which these techniques may be useful will concern quantitative studies of mixed-valence and heavy-fermion materials, for which the $4f$ and $5f$ orbital and spin magnetization densities are presently uncertain.

In Sec. V, we report measurements of the degree of linear polarization of the scattering obtained at several different chemical and magnetic reflections of holmium for incident x-ray energies set about 200 eV below the $L_{\rm III}$ absorption edge. We find that, for predominantly σ-polarized incident radiation, the radiation scattered at the chemical reflections is predominantly σ polarized, while that obtained at the magnetic reflections is predominantly π polarized (rotated by 90°). These results are consistent with calculations of the nonresonant cross section (derived in the high-energy limit) for charge and magnetic scattering.[14] The fact that the incident linear polarization vector is rotated upon magnetic scattering may be interpreted within the nonresonant limit as reflecting the large orbital moment in holmium. We have also made estimates of the magnitude of the resonant contributions to the σ- and π-polarized components of the magnetic scattering from the nearby $L_{\rm III}$ edge, and found that, while significant, these corrections appear to fall within the experimental error.

In the resonant regime, when the incident x-ray energy is tuned near an absorption edge, there are additional contributions to the x-ray-scattering cross section.[1-3] Within a one-electron view of the electronic structure, the incident photon promotes an inner shell electron to an unoccupied orbital above the Fermi energy, which subsequently decays through the emission of an elastically scattered photon. The amplitude for resonant magnetic scattering then depends on the matrix elements which couple the ground state and the excited magnetic states allowed by the exclusion principle. In this way, the energy and polarization dependence of the magnetic scattering probes the fine structure of magnetic states. It follows that detailed modeling of the line shapes of the magnetic scattering may reveal the spectrum of allowed transitions near E_f, including, perhaps, the magnitude of the exchange splitting and the induced polarization within metallic conduction bands.[2,3] It is also important to note that the polarization dependence of the resonant cross section depends in a simple way on the directions of the local atomic moments. The existence of large resonant enhancements of the magnetic scattering then makes feasible the determination of magnetic structures by x-ray-scattering techniques in a wider class of materials than was previously imagined. We believe that resonant techniques will be of special interest in studies of the magnetic properties of rare earths and actinides, particularly in application to multilayers, thin films, and surface layers. Experiments of this type are straightforward using synchrotron radiation when the incident x-ray energy lies near the L absorption edges of the rare earths ($\hbar\omega \sim 6$–10 keV) and the M absorption edges of the actinides ($\hbar\omega \sim 3$–5 keV). X-ray-reflectivity studies of these materials, and of transition elements, over an even wider range of energies offer still another direction for resonant studies of magnetic properties.

In Sec. VI, we confirm the approximately fiftyfold resonant enhancement of the x-ray magnetic scattering for the $(0,0,2+\tau)$ magnetic reflection of holmium for incident x-ray energies tuned near the $L_{\rm III}$ absorption edge, and characterize the energy dependence of the resonant second-, third-, and fourth-order harmonics.[1-3] We have also performed detailed measurements of the line shapes of the linearly σ- and π-polarized components of the magnetic scattering for the $(0,0,2+\tau)$, $(0,0,4+\tau)$, and $(0,0,6+\tau)$ magnetic reflections, and of their sum, both near to and about 150 eV below the $L_{\rm III}$ absorption edge. These line shapes have been fit to a simple model of the resonant cross section for a magnetic spiral, including electric dipole and quadrupole transitions, coupling $2p$ to $5d$ and $4f$ magnetic states, respectively.[2,3] Although not unique, the fits provide a reasonable description of the data, which is qualitatively consistent with an atomic orbital description of the electronic structure. The most significant feature of the line shapes is their pronounced asymmetry, which results from the interference of the resonant and nonresonant contributions to the cross section. We have also performed high-Q-resolution measurements of the profiles of the magnetic scattering as a function of the incident x-ray energy near the $L_{\rm III}$ edge, and found a slight broadening of the radial and transverse profiles, which we suggest is related to the increased absorption. In addition, we have measured the temperature dependence of the principal resonant and nonresonant magnetic cross sections for the $(0,0,2+\tau)$ reflection and found that, to within our statistics, they are identical. Finally, resonant magnetic scattering has been observed near the $L_{\rm II}$ and $L_{\rm I}$ absorption edges with an intensity which is considerably reduced from that observed at the $L_{\rm III}$ edge.

Before turning to a detailed discussion of our results for holmium, we note the results of some related efforts. Recently, experiments sensitive to the orbital- and spin-magnetization densities have been attempted in UAs,[16,17] and in Fe, Gd, and Tb.[18] Resonant and off-resonant x-ray magnetic scattering studies have been performed on most of the heavy rare-earth metals, including Ho,[1,9-11] Dy,[19] Tm,[20] and Er,[21] on two rare-earth magnetic multilayers, including Gd-Y (Ref. 22) and Ho-Y,[23] and in a variety of actinides and transition metals including UAs,[16,17] UN,[24] $\rm URu_2Si_2$,[25] $\rm UO_2$,[26] USb,[26] Ni,[27] $\rm MnF_2$,[28] and Fe.[29] The largest resonant enhancements have been observed for incident x-ray energies near the $M_{\rm IV}$ absorption edges of the actinides[16,17,24-26] and near the $L_{\rm III}$ absorption edges of the rare earths[1,19-21] and transition metals.[29] Spin-dependent absorption measurements have been performed on a wide variety of transition-metal and rare-earth powdered ferromagnets (see, for example, Ref. 30). Recently, calculations have been made of the resonant cross sections for scattering and for absorption in ferromagnets.[31]

The first x-ray magnetic scattering experiments were performed by deBergevin and Brunel on NiO and various Fe compounds,[32,33] following the original calculations of Platzman and Tsoar,[34] in 1972. The first polarization-sensitive x-ray magnetic scattering experiments were performed by Brunel and co-workers on Fe in 1982.[35] Blume suggested that interesting magnetic effects might occur near an absorption edge in 1985.[13] Namikawa and co-workers performed early measurements of resonant magnetic effects in Ni.[27]

The outline of this paper is as follows. The experimental procedures are summarized in Sec. II. Relevant features of the electronic and magnetic structure of holmium are described in Sec. III. Detailed expressions for the resonant and nonresonant contributions to the x-ray-scattering cross section are discussed for holmium in Sec. IV. The results of the experiments obtained off resonance and near resonance are presented and analyzed in Secs. V and VI, respectively.

II. EXPERIMENT

The experiments described in this paper were begun on beamline A-2 at the Cornell High Energy Synchrotron Source (CHESS) and continued on beamline X22C at the National Synchrotron Light Source (NSLS). For simplicity of presentation, we shall describe our procedures at NSLS X22C, elaborating only where necessary on particular aspects of the measurements performed at CHESS.

X22C utilizes a doubly focusing nickel-coated mirror (spot size ~ 1 mm^2) and a fixed-exit Ge(111) double-crystal monochromator. With this monochromator, the incident x-ray energy is tunable from about $\hbar\omega = 3$ to 30 keV, with an energy resolution between 5 and 10 eV at $\hbar\omega = 8067$ eV. The high-symmetry faces of a ($9\times4\times4$ mm^3) holmium sample were first mechanically polished, and then electropolished in a passivating methanol-perchloric solution.[36] The mosaic width measured at the chemical (0,0,2) reflection was 0.03°. The sample was supported inside a closed-cycle helium refrigerator and studied with the (0,0,L) face mounted in a vertical reflection geometry. NaI scintillation detectors were used to count the incident and scattered photons.

A schematic view of the geometry used in these experiments is shown in Fig. 1. In the figure, the x-ray beam is incident onto the sample from the left, and makes an angle θ with respect to its surface and to the $(0,0,L)$ Bragg planes. The coordinate system is chosen so that the σ-polarized components of the incident and scattered beams are normal to the diffraction plane (spanned by the incident and scattered wave vectors $\mathbf{k}$ and $\mathbf{k}'$), while the π-polarized components lie within the diffraction plane.

Linear polarization analysis was accomplished by means of an instrument which has been described in detail elsewhere.[37] Briefly, a pyrolytic-graphite (PG) crystal (with a mosaic width of 0.3°) was placed after the sample on the 2θ arm of the spectrometer. When the incident x-ray energy is tuned to $\hbar\omega = 7847$ eV, the scattering angle for the PG (0,0,6) chemical reflection is precisely 90° (θ_{graphite}, in Fig. 1). Consequently, one linear component of the beam scattered from the sample is reflected into the detector, while the other is suppressed. By accurately rotating the graphite analyzer assembly and detector about the axis of the scattered beam (ϕ_{poln}, in Fig. 1), the former is suppressed and the latter is reflected. In this way, the intensities of the linearly σ- and π-polarized components of the scattered beam may be independently measured. It is important to add that, while polarization analysis using the PG (0,0,6) reflection is optimally efficient at an energy $\hbar\omega = 7847$ eV, this same reflection may be used to analyze the polarization of the scattered beam in a range of energies several hundred eV around $\hbar\omega = 7847$ eV. For example, when the incident x-ray energy is tuned near the L_{III} absorption edge at $\hbar\omega = 8067$ eV, the difference in θ_{graphite} from 90° (see Fig. 1) leads to an error in the intensity of order 1%, which is neglected here. Using this device, the degree of linear polarization

$$P = (I_\sigma - I_\pi)/(I_\sigma + I_\pi)$$

of the incident beam was determined to be $P = 0.9 \pm 0.1$ on beamline X22C at NSLS and $P = 0.77 \pm 0.075$ on beamline A-2 at CHESS. These values are the averages obtained from measurements of the polarization of the direct beam, as well as of the charge scattering from the (0,0,2), (0,0,4), and (0,0,6) chemical Bragg reflections.

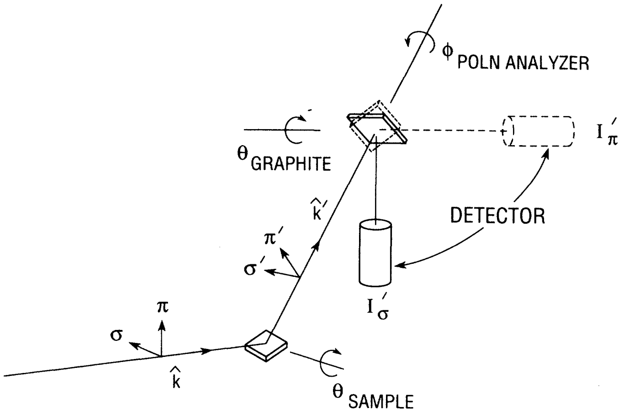

FIG. 1. Schematic view of geometry used in these experiments.

All of the results reported in this paper for the degree of linear polarization and for the energy dependence of the magnetic scattering were derived from integrated intensities, obtained by rocking the sample at the appropriate Bragg angles. It is noteworthy in this regard that the background intensities measured at each x-ray energy mirror the sample fluorescence, and thereby provided continuous, on-line calibration of the incident x-ray energy. Horizontal and vertical slits (located upstream of the mirror) were employed in order to symmetrize the divergence of the beam scattered from the sample.

Specifically, the horizontal and vertical divergences were set equal to about 0.03° at $2\theta = 35°$, which is about ten times smaller than the PG (0,0,6) mosaic width. As a result, it was not necessary when rocking the sample to also rock θ_{graphite} (in Fig. 1) at each θ_{sample} in order to obtain properly integrated intensities. Horizontal and vertical slits (located after the monochromator) were also used to limit the beam spot on the sample, thereby permitting the intensities obtained at large and small scattering angles to be directly compared (after correction by the Lorentz factor).

III. MAGNETIC STRUCTURE OF HOLMIUM

Metallic holmium has a hcp crystal structure with two layers per chemical unit cell and a saturation magnetic moment of $10.3\mu_B$/atom.[38] In the ground state there are ten $4f$ electrons in a Hund's-rule $^5I_8$ configuration and three electrons in the $5d$ and $6s$ bands. In the metal, the $5d$ and $6(s\text{-}p)$ conduction bands have energy widths between 5 and 10 eV, which is typical of rare earths.[39,40] The $4f$ bands have energy widths of about 2 eV and lie less than 5 eV above or below the Fermi energy.[39] In holmium, the L_{III} absorption edge occurs at $\hbar\omega = 8067$ eV, and is well separated from its L_{II} and L_{I} partners at $\hbar\omega = 8916$ and 9395 eV, respectively. The M_{IV} and M_{V} absorption edges occur at $\hbar\omega = 1392$ and 1351 eV, respectively.

Immediately below the magnetic ordering temperature ($T_N = 138$ K), the nonresonant x-ray (neutron) magnetic diffraction pattern for holmium consists of single pairs of magnetic satellites split symmetrically around each of the main chemical (nuclear) Bragg reflections, and parallel to the $[0,0,L]$, or c, axis. This pattern is consistent with a simple spiral modulation in which the average moments are ferromagnetically aligned within the basal planes, but rotate from plane to plane with an average turn angle proportional to the magnetic wave vector τ.[4,5,7,8] As the temperature is decreased from $T = 138$ K, the magnetic wave vector decreases from about $\tau \sim 0.3c^*$ to $\tau = \frac{1}{6}c^*$ below $T = 20$ K, and may lock to rational values.[7-12] At $T_c = 20$ K, there is a first-order transition to a conical magnetic structure with a net ferromagnetic moment along the c axis.

Besides the principal magnetic scattering at τ, weak fifth- and seventh-order harmonics have been observed below $T \sim 80$ K by neutron diffraction.[4,5,7-12] The distortions of the spiral implied by fifth and seventh harmonics result from the tendency of the atomic moments to bunch along the six easy directions defined by the basal-plane crystal field. Second- and higher-integral-order magnetic satellites have also been observed along the $[1,0,L]$ axis by neutron scattering.[4-12]

In early x-ray-scattering experiments on holmium, Keating[6] discovered additional charge scattering at $(1,1,L+2\tau)$, and attributed its origin to the asphericity of the $4f$ charge distribution. These peaks are not expected along the c axis for a simple spiral magnetic structure,[6] nor to our knowledge have they been observed. In high-resolution x-ray-scattering experiments, still more satellites (due to charge scattering) were discovered along the c axis and shown to arise from lattice modulations accompanying magnetic ordering.[9-11] These peaks reflect correlations among localized spin defects, or spin slips, and possess a wave vector satisfying the simple relation, $\tau_{\text{slip}} = 12\tau - 2$. More recently, nonintegral magnetic harmonics have been observed in holmium both along and off the c axis by neutron scattering, and a generalized phase discommensuration model has been applied to holmium.[12,41] In the experiments discussed in this paper, we are mainly concerned with the resonant and off-resonant magnetic scattering observed at $(0,0,L+\tau)$ (with L even), and with resonant harmonics observed at $(0,0,L+2\tau)$, $(0,0,L+3\tau)$, and $(0,0,L+4\tau)$. To our knowledge, no previous studies have reported harmonics at 2τ, 3τ, and 4τ along the c axis.

IV. X-RAY SCATTERING CROSS SECTION

A. Nonresonant amplitude

The cross section for elastic scattering of x-rays from a single crystal has the form

$$\frac{d\sigma}{d\Omega} = \left[\frac{e^2}{mc^2}\right]^2 \left|\sum_n^{\text{all atoms}} e^{i\mathbf{Q}\cdot\mathbf{R}_n} f_n(\mathbf{k},\mathbf{k}';\hbar\omega)\right|^2 , \qquad (1)$$

where R_n is the position of the nth atom in the crystal, $\hbar\omega$ is the incident photon energy, and $Q = k - k'$ is the photon momentum transfer. Using second-order perturbation theory, Blume[13] has shown that the scattering amplitude per atom f_n may be written

$$f_n(\mathbf{k},\mathbf{k}';\hbar\omega) = f_n^{\text{charge}(0)}(\mathbf{Q}) + f_n'(\mathbf{k},\mathbf{k}';\hbar\omega) + if_n''(\mathbf{k},\mathbf{k}';\hbar\omega) + f_n^{\text{spin}}(\mathbf{k},\mathbf{k}';\hbar\omega) , \qquad (2)$$

where $f_n^{\text{charge}(0)}$ is the usual Thomson contribution, f_n' and if_n'' are the contributions arising from $\mathbf{A}\cdot\mathbf{P}$, and f^{spin} represents the amplitude for all scattering which explicitly contains the electron-spin operator. In the limit of high-x-ray energies ($\hbar\omega \gg$ energy of any absorption edge), the scattering amplitude f_n may be simplified:[13-15]

$$f_n(\mathbf{k},\mathbf{k}';\hbar\omega) = f_n^{\text{charge}(0)}(\mathbf{Q}) + f_n^{\text{magnetic}(0)}(\mathbf{Q}) ,$$

where

$$f_n^{\text{charge}(0)}(\mathbf{Q}) = \rho_n(\mathbf{Q})\hat{\mathbf{e}}\cdot\hat{\mathbf{e}}'$$

and

$$f_n^{\text{magnetic}(0)}(\mathbf{Q}) = \frac{i\hbar\omega}{mc^2}[\tfrac{1}{2}\mathbf{L}_n(\mathbf{Q})\cdot\mathbf{A} + \mathbf{S}_n(\mathbf{Q})\cdot\mathbf{B}] . \qquad (3)$$

Here, $f_n^{\text{charge}(0)}$ and $f_n^{\text{magnetic}(0)}$ are the nonresonant amplitudes for charge and magnetic scattering, respectively. $\rho_n(Q)$ is the Fourier transform of the electronic charge density, and $\mathbf{L}_n(\mathbf{Q})$ and $\mathbf{S}_n(\mathbf{Q})$ are the respective Fourier transforms of the orbital- and spin-magnetization densities of the nth atom. $\hat{\mathbf{e}}$ and $\hat{\mathbf{e}}'$ are, respectively, the incident and final photon polarization vectors. The vectors $\mathbf{A}$ and $\mathbf{B}$ depend on the initial and final photon polarization vectors and on the initial and final photon wave vectors. General expressions for the vectors $\mathbf{A}$ and $\mathbf{B}$ may be found in Ref. 14.

For the particular case of a magnetic spiral, the degree of linear polarization of the scattered beam at the magnetic wave vector τ in the nonresonant limit is[14,42]

$$P'_m = \frac{I'_\sigma - I'_\pi}{I'_\sigma + I'_\pi} ,$$

where

$$I'_\sigma \propto (1+P) + (1-P)(1+g)^2 \sin^2(\theta) ,$$

$$I'_\pi \propto (1+P)(1+g)^2 \sin^2(\theta) + (1-P)[1+2g\sin^2(\theta)]^2 ,$$

and

$$g(\mathbf{Q}) = \frac{\mathbf{L}(\mathbf{Q})\cdot\mathbf{J}(\mathbf{Q})}{\mathbf{S}(\mathbf{Q})\cdot\mathbf{J}(\mathbf{Q})} = \frac{(\mathbf{L}\cdot\mathbf{J}) f_L(\mathbf{Q})}{(\mathbf{S}\cdot\mathbf{J}) f_S(\mathbf{Q})} . \tag{4}$$

In these expressions, the linearly σ- and π-polarized components of the photon polarization are taken to be, respectively, perpendicular to and coplanar with the x-ray-diffraction plane (see Fig. 1). θ is one-half the scattering angle and P is the incident degree of linear polarization. $g(\mathbf{Q})$ is the ratio of the orbital- and spin-magnetization densities, each projected along the total angular momentum. For holmium, $g(\mathbf{Q})$ may be rewritten in terms of the normalized orbital and spin form factors:[43] $g(\mathbf{Q}) = 3f_L/f_S$. It has also been assumed in writing Eq. (4) that the contributions from the right and left circularly polarized components of the incident beam cancel in the scattered beam. For this assumption to be valid, the magnetization across the surface must be uniform, the right and left circularly polarized components of the incident beam must have equal intensities, and all the scattered photons must be collected at the detector.

It is clear from Eq. (4) that, in the nonresonant limit, the degree of linear polarization for the x-ray magnetic scattering from a spiral is sensitive to the orbital- and spin-magnetization densities. Thus, by measurement of P', it should be possible to distinguish these contributions in x-ray-scattering experiments. In particular, it should be noted that, in the limit $P \rightarrow 1$, the σ-polarized component of the magnetic scattering from a spiral depends only on the spin-magnetization density ($I'_\sigma \propto |\mathbf{S}(\mathbf{Q})|^2$), while the π-polarized component depends on the sum of the orbital and spin densities

$$I'_\pi \propto |\mathbf{L}(\mathbf{Q}) + \mathbf{S}(\mathbf{Q})|^2 \sin^2\theta .$$

Since $P \sim 1$ in these experiments, it follows that the principal differences measured for the intensities of the σ- and π-polarized components of the magnetic scattering must originate in the contributions of the orbital-magnetization density of holmium.

The nonresonant degree of linear polarization of the charge scattering from the chemical structure is[14]

$$P'_{\mathrm{charge}} = \frac{1-\cos^2(\theta) + P[1+\cos^2(\theta)]}{1+\cos^2(\theta) + P[1-\cos^2(\theta)]} . \tag{5}$$

B. X-ray resonance exchange scattering

When the incident x-ray energy is tuned near an absorption edge, there are additional resonant contributions to the x-ray magnetic scattering amplitude.[1–3,13] In the following, we consider only the resonant terms arising from the operator $\mathbf{A}\cdot\mathbf{P}$ in the Hamiltonian, which contribute directly to f' and f'', and we ignore crystal-field effects.[1–3,13] An important consequence of such a simple description is that conventional electric multipole selection rules may be used to investigate which transitions are allowed. For the particular case of electric $2L$-pole (EL) transitions in a magnetic ion, the contribution to the coherent scattering amplitude from $\mathbf{A}\cdot\mathbf{P}$ may be written[2,3]

$$f_{EL} = 4\pi\lambda \sum_{M=-L}^{L} [\hat{\mathbf{e}}'^{*}\cdot Y_{LM}(\hat{\mathbf{k}}') Y^{*}_{LM}(\hat{\mathbf{k}})\cdot\hat{\mathbf{e}}] F_{LM}(\omega) ,$$

where

$$F_{LM}(\omega) = \sum_{a,b} \frac{P_a P_{a(b)} \Gamma_x(aMb;EL)/\Gamma}{X(a,b) - i} . \tag{6}$$

In this expression, the Y_{LM}'s are the vector spherical harmonics with quantization axis $\hat{\mathbf{Z}}_J$, $\hat{\mathbf{k}}$ and $\hat{\mathbf{k}}'$ are the initial and scattered photon wave vectors, and λ is the photon wavelength. a and b are the initial and excited ionic states of energy E_a and E_b, respectively. P_a gives the statistical probability for the initial state a, and $P_{a(b)}$ gives the probability that the excited state b is vacant for transitions from a. Summed over M, $\Gamma_x(aMb;LM)$ gives the partial width for EL radiative decay from the b to a, and Γ is the total width for b (determined from all radiative and nonradiative decay). In the resonance denominator,

$$x(a,b) = 2(E_a - E_b - \hbar\omega)/\Gamma .$$

It is clear from Eq. (6) that the amplitude of the resonant scattering is determined by the detailed electronic structure through the F_{LM}'s. Specifically, the energy widths Γ_x and Γ depend directly on matrix elements of the initial and excited states.[2,3] Provided sufficient spin-orbit correlations among the ground or resonant states that the sums on M are nonzero,[2,3] it follows that the greater the overlap is of the wavefunctions, the greater the resonant magnetic intensity will be. For this reason, the L and M absorption edges of the rare earths and actinides (for which the overlap is large) have been studied intensively. It also follows from Eq. (6) that the polarization dependence of the resonant scattering is determined independently of the F_{LM}'s through the dependence of the vector spherical harmonics (Y_{LM}) on the direction of the local ionic moment $\hat{\mathbf{Z}}_J$. Further, the spectrum of the allowed diffraction harmonics ($m\tau$, $m=0$, 1, 2, etc.) arises from the dependence of the Y_{LM} products on powers of $\hat{\mathbf{Z}}_J$.

For incident x-ray energies near the L_{III} absorption edge of holmium, the dominant contributions to the resonant scattering [Eq. (6)] arise from (1) electric dipole transitions coupling $2p$ core and $5d$-derived conduction-band states, and (2) electric quadrupole transitions coupling $2p$ and $4f$-derived states. (Transitions involving $6s$ states are ignored by virtue of the assumed small induced s moment and the small overlap with the p states.) For core excita-

TABLE I. Polarization dependence of x-ray-scattering cross section from a magnetic spiral for $E1$ and $E2$ transitions, assuming σ-polarized incident radiation (Refs. 2 and 3).

Harmonic	$E1$	$E2$
0	σ	σ
1	π	σ,π
2	σ,π	π,σ
3	none	σ,π
4	none	σ,π

tions involving typical x-ray energies between $\hbar\omega=5$ and 10 keV, a reasonable first step is to assume that one-particle Hartree-Fock wave functions provide an adequate description of the electronic structure. In the following, the initial state of the resonant electron in holmium is taken to be an atomic $2p$ state:

$$|2p_{\frac{3}{2}},m_j\rangle \text{ with } m_j=-\tfrac{3}{2},\ -\tfrac{1}{2},\ \tfrac{1}{2},\text{ and } \tfrac{3}{2}\ .$$

Similarly, the states within the $5d$ band are assumed to be

$$|5d,m_l,m_s\rangle \text{ with } m_1=-2,\ -1,\ 0,\ 1,\text{ and } 2$$

and

$$m_s=\pm\tfrac{1}{2}\ .$$

It may be further assumed that the spin-down and spin-up holes differ in energy by the exchange splitting Δ, and that the energy of the spin-down holes lies lowest. The consequences of this assumption for the line shapes observed in holmium are discussed in Sec. VI A. The four $4f$ holes available in a quadrupole transition are taken to be

$$|4f,m_l,m_s\rangle \text{ with } m_l=-3,\ -2,\ -1,\text{ and } 0$$

and

$$m_s=-\tfrac{1}{2}\ .$$

The linear polarization dependence and the spectrum of allowed diffraction harmonics may also be calculated for a magnetic spiral.[2,3] Assuming purely σ-polarized incident radiation, there are two resonant harmonics for the electric dipole scattering and four for the electric quadrupole scattering. The detailed polarization dependence is shown in Table I.

Hannon *et al.*[2,3] have computed the relative intensities expected for each of the harmonics listed above from explicit calculations of the F_{LM}'s, using $2p$, $5d$, and $4f$ atomic wave functions of $(\mathrm{Ho})^{3+}$. In addition, they have considered the corresponding intensities for the $(2p\rightarrow 5d,\ 2p\rightarrow 4f)$ and $(2s\rightarrow 6p,\ 2s\rightarrow 5d,\ 2s\rightarrow 4f)$ transitions appropriate for the respective L_{II} and L_{I} absorption edges. We refer to the results of these calculations as needed in the following.

V. OFF-RESONANT REGIME

In this section we report the results of measurements of the degree of linear polarization P' of both charge and magnetic scattering along the c axis for an incident x-ray energy of $\hbar\omega=7847$ eV. This value of the energy lies about 200 eV below the energy of the L_{III} absorption edge, and was chosen so that the PG(0,0,6) reflection used to analyze the final polarization had a scattering angle (θ_{graphite} in Fig. 1) of precisely 90°. Our goal in these experiments was to identify the orbital and spin contributions to the magnetization density through the use of Eq. (4) for nonresonant magnetic scattering.

Figure 2 shows the results of rocking the sample through each of the chemical Bragg reflections at (0,0,2), (0,0,4), and (0,0,6) for the σ- and π-polarized components of the charge scattering. These scans, and those shown in Fig. 3, were made with the sample held at a temperature $T<20$ K, in which holmium exhibits a conical magnetic structure with $\tau=\frac{1}{6}c^*$. It is clear from Fig. 2 that for each reflection the intensity of the σ-polarized component of the charge scattering is considerably stronger than that of the π-polarized component. This behavior reflects the profile of the incident beam, which is predominantly σ polarized. Indeed, the integrated intensities obtained from these (and similar) scans were combined with the results obtained from direct measurements of the incident beam to determine the average incident degree of linear polarization. It is noteworthy that the decrease in intensity of the σ-polarized component observed with in-

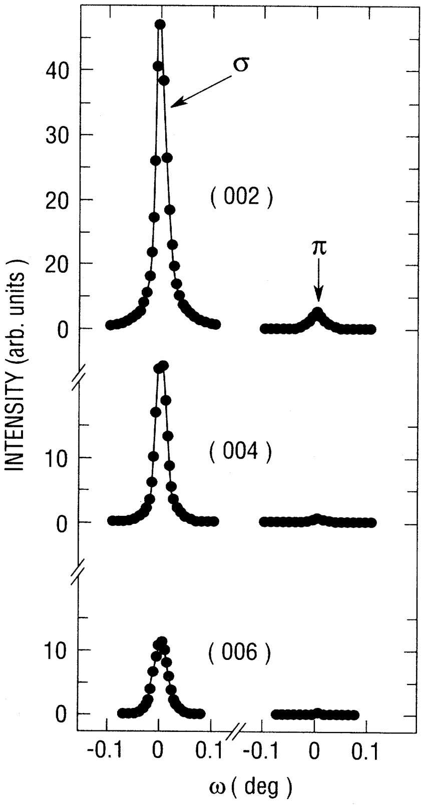

FIG. 2. Rocking curves of the σ- and π-polarized components of the charge scattering for the (0,0,2), (0,0,4), and (0,0,6) chemical reflections of holmium, obtained for an incident x ray of $\hbar\omega=7847$ eV.

creasing momentum transfer in Fig. 2 is consistent with calculations of the structure factor of holmium, after accounting for the form factor, Lorentz factor, and incident polarization.

Figure 3 shows the results of rocking the sample through each of the magnetic Bragg reflections at $(0,0,2+\tau)$, $(0,0,4+\tau)$, and $(0,0,6+\tau)$ for the σ- and π-polarized components of the magnetic scattering. In contrast to the results for the charge scattering shown in Fig. 2, the intensity of the π-polarized component of the magnetic scattering dominates the intensity of the σ-polarized component. Note also that the intensity of the π-polarized component increases with increasing momentum transfer, from the $(0,0,2+\tau)$ to the $(0,0,4+\tau)$, where it takes a maximum. Referring to the expression for the π-polarized component of the nonresonant cross section [Eq. (4)] and assuming $P \rightarrow 1$, it is seen that the dominance of the π-polarized component observed in the data reflects the existence of a large orbital moment in holmium. The observed Q dependence of the π-polarized component is qualitatively consistent with the decrease of $\sin(\theta)$ at small momentum transfers, and with the decrease of the orbital and spin form factors at large momentum transfers. Typical counting rates (obtained at CHESS) for the π-polarized component of the $(0,0,4+\tau)$ magnetic reflection at this energy were about 50 $\sec^{-1}$ on backgrounds of $<1 \sec^{-1}$ with a mosaic width of 0.03° (identical to the charge peaks). Background rates for the σ channel were larger, typically 5 $\sec^{-1}$, due to charge scattering.

The results shown in Fig. 2 and 3 are quantified in Fig. 4, where the degree of linear polarization of the charge and magnetic scattering is plotted versus the momentum transfer $\sin(\theta)/\lambda$. The solid square at $Q=0$ in Fig. 4 represents the degree of linear polarization of the incident beam $P=0.77$ (obtained at CHESS). The open circles show the degree of linear polarization P_c' of the charge scattering at the (0,0,2), (0,0,4), and (0,0,6) chemical Bragg reflections. The solid line drawn through the open circles gives the prediction of Eq. (5) for nonresonant charge scattering. The solid circles in Fig. 4 show the average degree of linear polarization P_m' mea-

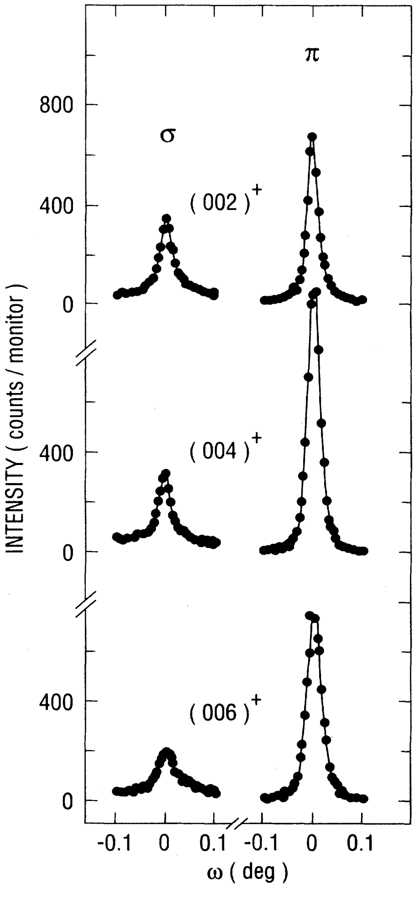

FIG. 3. Rocking curves of the σ- and π-polarized components of the x-ray magnetic scattering for the $(0,0,2+\tau)$, $(0,0,4+\tau)$, and $(0,0,6+\tau)$ magnetic reflections of holmium, obtained for an incident x-ray energy of $\hbar\omega=7847$ eV.

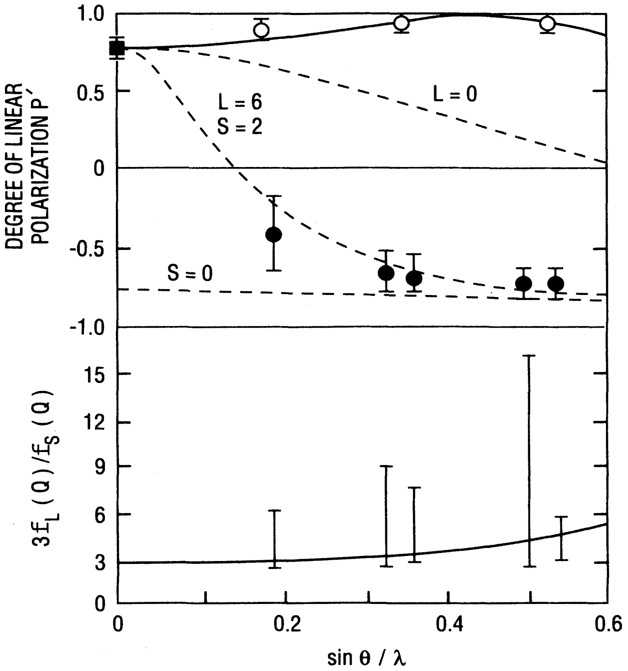

FIG. 4. Top: The solid square at $\theta=0$ corresponds to the degree of linear polarization of the incident beam. The open circles show the degree of linear polarization measured for the charge scattering and plotted vs momentum transfer for the (0,0,2), (0,0,4), and (0,0,6) chemical reflections. The solid line is degree of linear polarization for the charge scattering calculated from Eq. (5). The solid circles show the degree of linear polarization measured for the magnetic scattering at the $(0,0,2+\tau)$, $(0,0,4\pm\tau)$, and $(0,0,6\pm\tau)$ reflections. The dashed lines show the degree of linear polarization calculated from Eq. (4) for the nonresonant magnetic cross section assuming ($L=0, S$ arbitrary), ($L=6, S=2$), and (L arbitrary, $S=0$). Bottom: The brackets indicate the corresponding ratio $g(Q)$ of the orbital and spin form factors for the magnetic scattering obtained by inverting Eq. (4). The solid line gives $g(Q)$ calculated from Ref. 43.

sured for the positive and negative magnetic reflections at $(0,0,2+\tau)$, $(0,0,4\pm\tau)$, and $(0,0,6\pm\tau)$. The large error bars indicated for the magnetic scattering reflect the uncertainty arising from the larger background (due to charge scattering) which occurs in the σ channel of the scattered beam. The dashed line labeled $(L=6, S=2)$ shows the degree of linear polarization P'_m calculated from the nonresonant cross section, Eq. (4), assuming $L=6$ and $S=2$ and using calculated form factors for the Q dependence of the orbital- and spin-magnetization densities.[43] The remaining dashed lines show P'_m calculated from Eq. (5) assuming first ($L=0$ and S arbitrary), and then, (L arbitrary and $S=0$). It is clear from the figure that the predominantly σ-polarized character of the incident beam is preserved upon charge scattering ($P'_c>0$), but that the incident linear polarization is rotated upon magnetic scattering ($P'_m<0$). To within the experimental error, this behavior is consistent with the nonresonant cross sections for both the charge and the magnetic scattering. In terms of the nonresonant cross section for the magnetic scattering, this behavior reflects the fact that the orbital-magnetization density in holmium is large relative to the spin density, and that the π-polarized component of the intensity follows a sine-squared dependence on θ [see Eq. (4)].

The measured ratio $g(Q)$ of the orbital and spin form factors is compared to the ratio calculated using nonrelativistic Hartree-Fock wave functions[43] in the lower panel of Fig. 4. At $Q=0$, the calculated ratio (solid line) equals 3.0. At higher momentum transfer, the ratio increases, reflecting the rapid falloff of the form factor for spin in holmium. As may be seen, however, the experimental error spans this variation in Q.

It is noteworthy that the deviations of P'_m from predicted nonresonant behavior in the top panel of Fig. 4 appear the largest at small momentum transfers, near the $(0,0,2+\tau)$ reflection (where the error bars, unfortunately, are also largest). Attempts to measure the off-resonant degree of linear polarization for the magnetic satellites nearest to $Q=0$, where $P'_m>0$ is predicted by Eq. (4), have so far been unsuccessful. (These satellites have been successfully observed at resonance, however.) This is probably due to the fact that, at small momentum transfers, only a fraction of the incident beam actually impinges upon the sample, and that the background levels are large relative to the signal levels. More recently, we have measured the energy dependence of the magnetic scattering in holmium over several hundred eV around the L_{III} absorption edge, and fit the results to a simple resonant model of the x-ray cross section (see Sec. VI). These results permit semiquantitative estimates to be made of the magnitude of the resonant contributions to the total magnetic scattering at $\hbar\omega=7847$ eV. In particular, the calculations show that the resonant contributions to the intensities of the σ- and π-polarized components of the magnetic scattering may be as large as 20% of the nonresonant contributions for the $(0,0,2+\tau)$, $(0,0,4+\tau)$, and $(0,0,6+\tau)$ reflections (see inset, Fig. 12). Referring to Fig. 4, the addition of resonant contributions to the calculated P'_m would reduce it at small momentum transfers, but not to the point where it falls outside the experimental error bars. Similar calculations of the resonant contributions from the L_{II} and M_{IV} absorption edges suggest that these are negligible at $\hbar\omega=7847$ eV.

We conclude from this discussion that the present results, obtained about 200 eV below the L_{III} absorption edge, are consistent with the qualitative features of the nonresonant cross section predicted for a magnetic spiral, and, in particular, with the existence of a large orbital moment in holmium. The agreement is preserved (to within the error bars) when semiquantitative estimates of the resonant magnetic cross section are also included. More generally, it seems clear that both resonant and nonresonant contributions to the magnetic cross section must be explicitly considered in experiments which seek to determine the atomic orbital- and spin-magnetization densities. Significant improvement of the experimental results is possible by the increase of the signal-to-noise ratio in the σ channel of the polarization analyzer, and by the increase of the degree of linear polarization of the incident beam $P\rightarrow 1$ [see Eq. (4)].

VI. RESONANT REGIME

A. L_{III} absorption edge

Representative rocking curves of the $(0,0,2+\tau)$ magnetic reflection, obtained as the incident photon energy is tuned through the L_{III} absorption edge, are shown in Fig. 5. In these scans the sample temperature was fixed at $T=32$ K, at which temperature holmium exhibits a simple spiral magnetic phase with $\tau=0.189c^*$. The data in Fig. 5 were obtained without the use of an analyzing crystal. Instead, two sets of horizontal and vertical slits were located on the 2θ arm with slit separations of about 5 mm each. The results for $\hbar\omega=8000$ eV are shown in the lower right of the figure, where a small magnetic peak is visible on top of a flat background. Typical count rates in the magnetic peak at this energy were about 1000 sec^{-1} (on backgrounds of about 1 sec^{-1}) at an NSLS electron storage-ring current of 100 mA. As the incident photon energy is increased, the scattering angle (2θ) decreases and the peak intensity increases, until about $\hbar\omega=8070$ eV, where the magnetic intensity reaches a maximum. At this energy the measured count rate in the magnetic peak is about 45 000 sec^{-1} (at a ring current of 100 mA) on a background of about 2000 sec^{-1}. Thus, the measured peak intensity increases by nearly a factor of 50 by tuning the incident x-ray energy from $\hbar\omega=8000$ eV to an energy near the L_{III} absorption edge. Relative to the intensity of the charge scattering obtained at the $(0,0,2)$ reflection, the resonant magnetic scattering at the $(0,0,2+\tau)$ reflection is reduced by a factor of order 10^4. The increased background above the edge originates in the holmium L_{III} fluorescence, and may be reduced by the use of an energy dispersive detector. Above $\hbar\omega=8070$ eV, the magnetic intensity again decreases but remains on top of the large fluorescent background.

Integrated intensities measured for the $(0,0,2+\tau)$ magnetic satellite are shown plotted on a linear scale from $\hbar\omega=7700$ eV to $\hbar\omega=8100$ eV in the lower part of Fig. 6. Although the intensity obtained near $\hbar\omega=7700$ eV (the lowest energy studied in these experiments) appears small when plotted on this scale, the measured signal at that energy was several hundred count/sec. The data in the figure have been corrected at each energy for the holmium L_{III} absorption, which is shown plotted in the top panel of Fig. 6. For simplicity, we have assumed the infinite flat plate geometry, in which the integrated intensity is multiplied by the absorption coefficient μ at each incident photon energy. To determine the absorption correction, the transmission through a 5-μm holmium film was measured under alignment conditions identical to those present in the scattering experiment. Referring to the figure, the width of the absorption is between 5 and 10 eV, and the inflection point of the abrupt change is located at $\hbar\omega = 8067$ eV. It is important to note that none of the qualitative features of the line shapes visible in the raw data are significantly altered by the absorption correction. After correction for the absorption, the integrated intensity measured at the L_{III} absorption edge for the $(0,0,2+\tau)$ reflection is greater by a factor of about 150 than the integrated intensity measured at $\hbar\omega = 7850$ eV.

In addition to the resonant enhancement observed for the magnetic scattering at $(0,0,L=2+\tau)$, we have also observed resonant harmonics of the magnetic scattering at $L=2+2\tau$, $2+3\tau$, and $2+4\tau$. The energy dependence of the integrated intensity, corrected for the absorption, of the resonant magnetic scattering at τ and its harmonics is shown plotted on a linear scale in Fig. 7. At the top of the figure are the results at τ. The maximum integrated intensity occurs a few eV above the inflection point of the absorption at an incident photon energy $\hbar\omega = 8070$ eV and the energy full width at half maximum (FWHM) is about 10 eV. The second panel of Fig. 7 shows the energy dependence of the scattering at 2τ. In this case, no scattering is observed below $\hbar\omega = 8040$ eV nor above $\hbar\omega = 8082$ eV. Similar to the magnetic scattering at τ, the maximum intensity again occurs near 8070 eV, but is reduced by a factor of about 25. In contrast to the scattering at τ, the line shape for the scattering at 2τ exhibits a shoulder near $\hbar\omega = 8062$ eV, which leads to a broadening of the FWHM to about 14 eV. (It is shown below that the profiles obtained at τ and at 2τ may each be decomposed into two peaks, split symmetrically above and below the inflection point of the absorption by about 6 eV.) The energy dependence of the integrated intensity of the scattering at $L=2+3\tau$ is shown in the third panel of Fig. 7. To within the experimental statistics, no scattering is observed below $\hbar\omega = 8054$ eV nor above $\hbar\omega = 8080$ eV. The profile of the scattering at 3τ takes a maximum at $\hbar\omega = 8063$ eV, which is about 4 eV below the inflection point of the absorption.[44] The energy FWHM for the

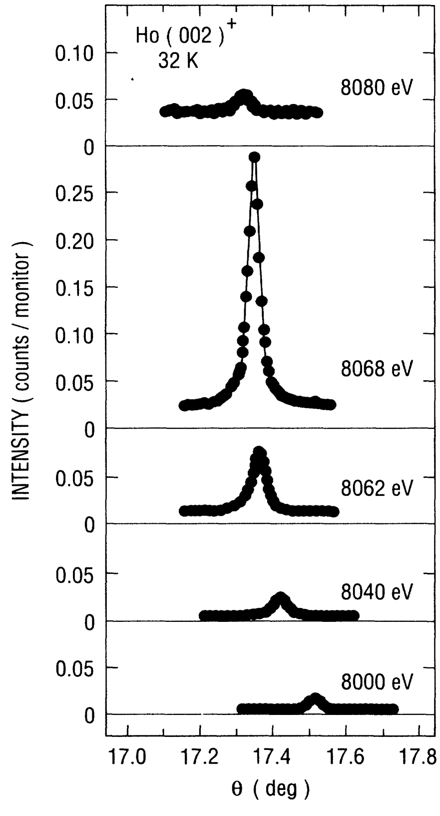

FIG. 5. Rocking curves of the x-ray magnetic scattering for holmium at the $(0,0,2+\tau)$ reflection plotted as the incident x-ray energy is tuned through the L_{III} absorption edge at $\hbar\omega = 8067$ eV.

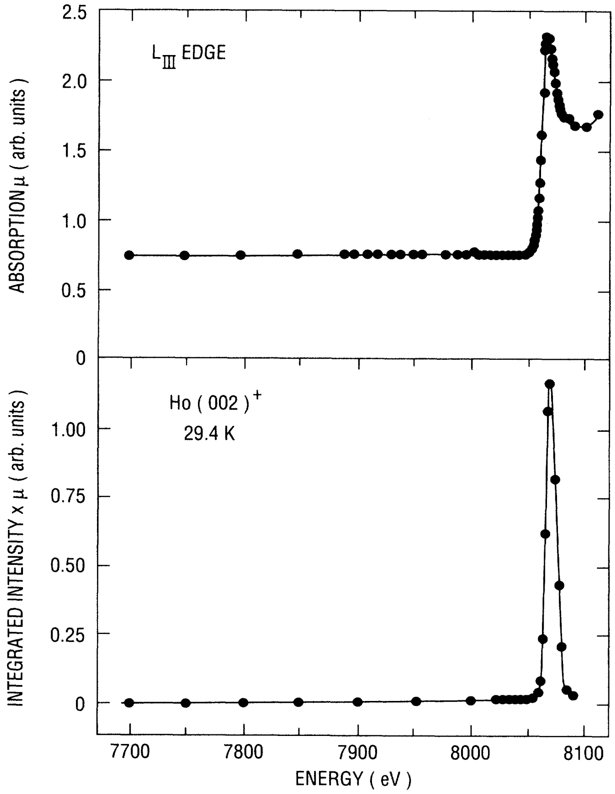

FIG. 6. Top: The absorption measured from a 5-μm holmium film as the incident x-ray energy is tuned through the L_{III} edge. Bottom: The integrated magnetic intensity of the $(0,0,2+\tau)$ reflection of holmium for the same range of incident photon energies. Solid lines are drawn only to guide the eye.

scattering at 3τ is 6 eV, which is the instrumental resolution at this incident-photon energy. The profile for the scattering at $L=2+4\tau$, shown in the fourth panel, also takes a maximum at $\hbar\omega=8063$ eV and has similar energy width.

The energy dependence of the linearly σ- and π-polarized components of the scattering observed at $4+\tau$, $2+2\tau$, and $2+3\tau$ is shown in Fig. 8. The top panel of the figure gives the measured absorption coefficient plotted as the incident x-ray energy is tuned through the L_{III} absorption edge. The solid vertical line indicates the inflection point of the abrupt change of the absorption located at $\hbar\omega=8067$ eV. In the lower panels, the open circles indicate the results obtained for the π-polarized components of the scattered beam, while the solid circles indicate the results obtained for the σ-polarized component. At each photon energy shown in the figure, the scattering angle of the polarization analyzer (θ_{graphite} in Fig. 1) was incremented, the sample orientation checked, and then the sample rocked through the appropriate Bragg angle in order to obtain properly integrated intensities.

Referring to the second panel of the figure, it is clear that the σ- and π-polarized components of the magnetic scattering have significantly different line shapes. In particular, the π-polarized component of the intensity takes

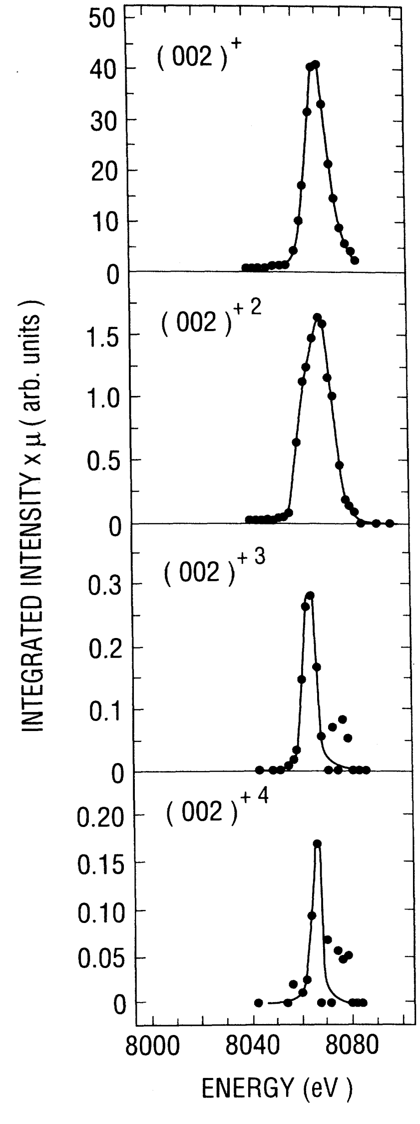

FIG. 7. Integrated magnetic intensity of the $(0,0,L=2+\tau)$ magnetic reflection and of its harmonics located at $L=2+2\tau$, $2+3\tau$, and $2+4\tau$, plotted as the incident x-ray energy is tuned through the L_{III} absorption edge. Solid lines are drawn only to guide the eye.

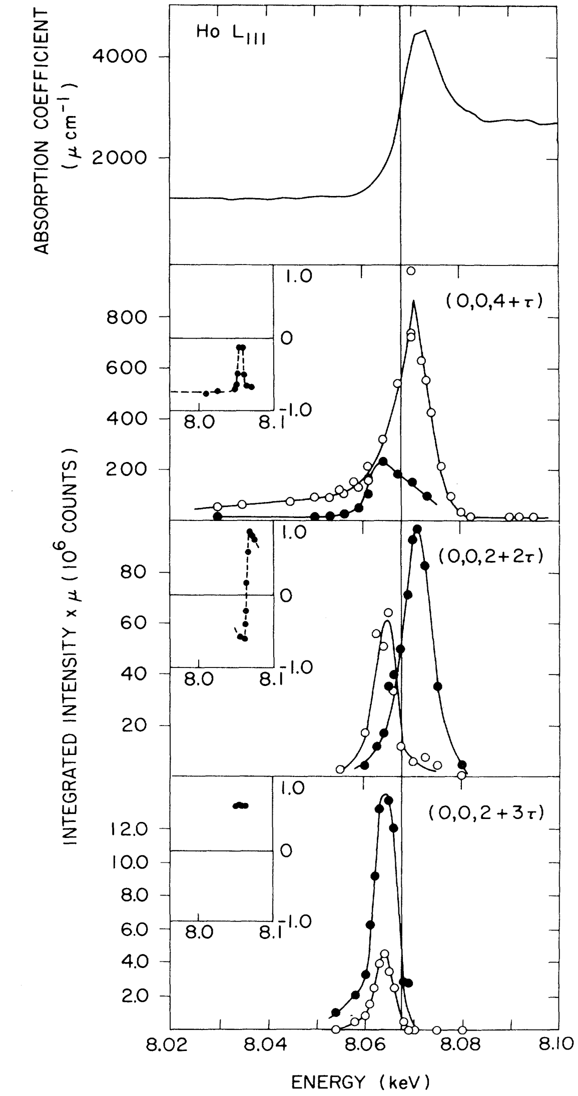

FIG. 8. Top: The absorption measured through a 5-μm holmium film plotted as the incident x-ray energy is tuned through the L_{III} edge. Bottom: Integrated magnetic intensities of the σ- (solid circles) and π- (open circles) polarized components of the scattering at the $(0,0,4+\tau)$, $(0,0,2+\tau)$, and $(0,0,2+3\tau)$ reflections. The solid lines are drawn only to guide the eye. Insets, bottom: Corresponding degree of linear polarization plotted vs energy. The solid vertical line indicates the energy of the inflection point of the L_{III} absorption edge.

a maximum about 3 eV above the inflection point of the absorption, while the σ-polarized component peaks about 3 eV below.[45] Further, the π-polarized component of the scattering appears asymmetric, with a long tail to lower energy. A similar asymmetry to higher energy is suggested by the σ-polarized component, but is not established by the data. In contrast to the behavior at τ, the π-polarized component of the scattering at 2τ, shown in the third panel, takes a maximum below the inflection point of the absorption and the σ-polarized component reaches a maximum above. At 2τ, neither line shape appears asymmetric to within the available statistics. For the scattering at 3τ, both components peak below the inflection point and no scattering is observed above. (A polarization analysis was not performed at 4τ.)

The degree of linear polarization P' for the scattering at each harmonic plotted versus incident photon energy is shown inset in Fig. 8. For the magnetic scattering at τ, P'_m undergoes a resonance near $\hbar\omega = 8062$ eV, suggesting that, at this energy, the scattering is mainly circularly polarized (or unpolarized). In contrast, the intensity of the scattering at 2τ is predominantly π polarized below the inflection point ($P' < 0$), and σ polarized above the inflection point ($P' > 0$). Evidently, the degree of linear polarization at 3τ is mainly σ polarized ($P' > 0$) and independent of the incident x-ray energy.

In our view, all of the data presented in Figs. 7 and 8 are most simply characterized by supposing that the energy dependence of the diffraction pattern is derived from two excitations, split below and above the inflection point of the absorption. In the excitation channel corresponding to x-ray energies below the inflection point, resonant scattering exists at four harmonics: τ, 2τ, 3τ, and 4τ. In the channel corresponding to x-ray energies above the inflection point, resonant scattering exists at only two harmonics, τ and 2τ, and is absent at higher harmonics. (No experiments were attempted at momentum transfers corresponding to fifth and higher harmonics.) This description of the data finds a natural explanation in the theory of x-ray resonance exchange scattering,[2,3] which has been summarized in Sec. IV. According to these ideas, both resonant and nonresonant contributions to the x-ray cross section may exist for incident x-ray energies near the L_{III} absorption edge. The nonresonant contributions depend on the atomic orbital- and spin-magnetization densities,[14] as has been discussed in Sec. V. The resonant contributions arise from electric multipole contributions to the x-ray scattering cross section. In application to holmium, it has been shown that the dipole-allowed transitions, coupling $2p$ core electrons with $5d$-derived conduction-band states, lead to only two harmonics: at τ and 2τ (see Sec. IV). Similarly, the quadrupole-allowed transitions, coupling $2p$ core electrons to $4f$-derived states, lead to four harmonics: at τ, 2τ, 3τ, and 4τ. It is then straightforward to associate the scattering observed above the inflection point of the absorption in Figs. 7 and 8 with the $2p \rightarrow 5d$ transitions and, similarly, to associate the scattering below the inflection point with $2p \rightarrow 4f$ transitions. Importantly, the observed polarization dependence of the resonant scattering at τ and its harmonics in Fig. 8 is consistent with the polarization dependence calculated for a magnetic spiral in Table I. For these reasons, and for others presented below, we find the description of the data offered by the theory of x-ray resonance exchange scattering to be convincing.

B. Energy dependence of the line shapes

To investigate the dependence of the line shapes on electric-multipole transitions, on the induced polarization and exchange splitting within the d band, and on the nonresonant magnetic scattering, systematic studies of the integrated magnetic intensity of the $(0,0,2+\tau)$, $(0,0,4+\tau)$, and $(0,0,6+\tau)$ magnetic reflections were undertaken between $\hbar\omega = 7900$ and 8150 eV. Results were obtained for the total cross section at τ, as well as for the σ- and π-polarized components of the magnetic scattering at τ. As in earlier sections, all of the intensities reported here are integrated intensities, and have been corrected for the absorption and by the Lorentz factor. Except for a single scale factor ($\mathcal{A}_1$, below), these intensities may be regarded as absolute. In the analysis, however, no account has been taken of the contributions to the scattering from nonlinearly polarized components of the incident or scattered beams. Although we believe these additional contributions are probably small ($P = 0.9 \pm 0.1$ at NSLS), they certainly exist, and they may distort the line shapes. For this reason, our interpretation of the line shapes is limited mainly to their qualitative features. It is worth noting in this regard that the degree of linear polarization P'_m partially escapes these difficulties by subtracting these contributions in its numerator. Unfortunately, measurements of the energy dependence of P'_m are limited in these experiments by the weakness of the σ-polarized component of the magnetic scattering (see Fig. 11). In the experiments described below, the sample temperature was fixed near $T = 32$ K, at which temperature holmium exhibits a spiral magnetic phase with $\tau = 0.189c^*$.

The total integrated intensity obtained at the magnetic wave vector τ for the $(0,0,2+\tau)$, $(0,0,4+\tau)$, and $(0,0,6+\tau)$ reflections is plotted on a logarithmic scale versus incident x-ray energy in Fig. 9. In these experiments, polarization analysis was not performed, and the detector was placed directly after the slits on the 2θ arm. For clarity of presentation, the results for the $(0,0,2+\tau)$ and $(0,0,4+\tau)$ reflections have been scaled by factors of 200 and 10, respectively. The solid lines in Figs. 9–11 are the results of fits, which are discussed below. The main features of the line shapes in Fig. 9 are clear. In each case the profile of the magnetic scattering exhibits a long, asymmetric tail which extends toward lower energy and a large enhancement of the scattering in the neighborhood of the L_{III} edge. The asymmetry is weakest, and the enhancement largest, for the $(0,0,2+\tau)$ satellite. As the scattering angle increases, the relative asymmetry also increases. It is interesting that the resonance width for the $(0,0,6+\tau)$ reflection is broader near the L_{III} edge than are the corresponding widths for the $(0,0,4+\tau)$ or $(0,0,2+\tau)$ reflections. This behavior, which is mirrored in the results for the π-polarized component of the magnetic scattering at high momentum transfers (shown in Fig. 10), suggests the possibility of additional fine structure. Above the $L_{\rm III}$ absorption edge, the scattering is again reduced, and the fluorescent background is large.

The linearly σ- and π-polarized components of the magnetic scattering from the $(0,0,2+\tau)$, $(0,0,4+\tau)$, and $(0,0,6+\tau)$ reflections are plotted on a linear scale versus incident x-ray energy from $\hbar\omega=7900$ to 8150 eV in Fig. 10. It is clear from the figure that for each reflection, the σ- and π-polarized components of the magnetic scattering have distinct line shapes, as found earlier for the $(0,0,4+\tau)$ reflection in Fig. 8. As before, the π-polarized component is dominant in each case and takes a maximum a few eV above the inflection point of the absorption. In addition, the π-polarized components each exhibit a long, asymmetric tail to lower energies and the asymmetry increases relative to the resonant maximum with increasing momentum transfer. In this regard, the line shapes for the π-polarized components are nearly identical to those obtained for the total magnetic scattering shown in Fig. 9. This reflects the weakness of the σ-polarized components of the intensity relative to the π-polarized components. The maximum intensity occurs for the $(0,0,2+\tau)$ reflection. After correction by the Lorentz factor, the maximum intensity for the $(0,0,4+\tau)$ reflection is slightly reduced relative to the $(0,0,2+\tau)$ reflection, and that for the $(0,0,6+\tau)$ reflection is reduced by about a factor 2.[46] In contrast, the intensities of the σ-polarized components of the magnetic scattering take a maximum about 2–3 eV below the inflection point of the absorption, and are reduced from the intensities of the π-polarized components by a factor 3–5. To within the available statistics, the maximum intensities for the σ-polarized components are all approximately equal. As was seen in Fig. 8, the line shapes of the σ-polarized components again suggest, but do not establish, the possibility of an asymmetry toward higher energies.

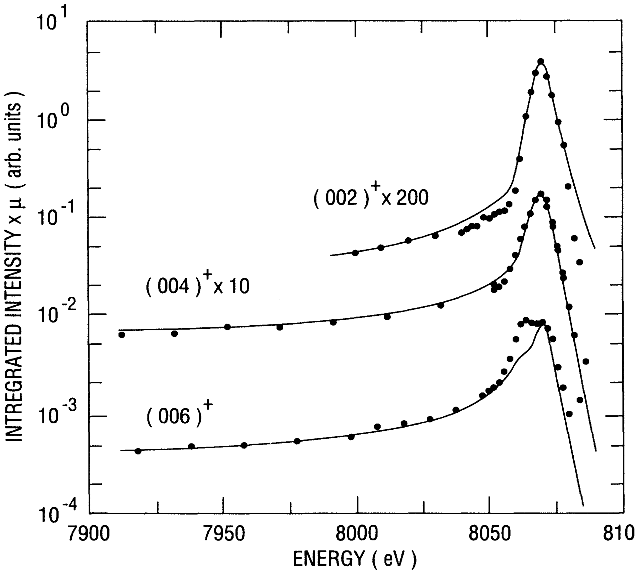

FIG. 9. Total integrated intensity for the $(0,0,2+\tau)$, $(0,0,4+\tau)$, and $(0,0,6+\tau)$ reflections plotted on a logarithmic scale as the incident x-ray energy is tuned through the $L_{\rm III}$ absorption edge. The solid lines are the results of fits, which are discussed in the text.

The degree of linear polarization for the magnetic scattering P'_m obtained for the $(0,0,2+\tau)$, $(0,0,4+\tau)$, and $(0,0,6+\tau)$ reflections is plotted in Fig. 11. In each case there is a resonance in P'_m near $\hbar\omega=8062$ eV. At this incident energy the quadrupole contributions to the resonant scattering (and, consequently, the σ-polarized components of the scattering at τ) are the greatest. This behavior is consistent with the earlier results for τ shown inset in Fig. 8, and with the polarization dependence of the cross section shown in Table I.

We have modeled the energy dependence of the magnetic scattering for the $(0,0,2+\tau)$, $(0,0,4+\tau)$, and $(0,0,6+\tau)$ reflections, using Eqs. (3) and (6) for the nonresonant and resonant x-ray-scattering amplitudes, respectively. In the model, we assume that the resonant contributions to the π-polarized components of the cross section arise mainly from electric-dipole transitions coupling $2p$ core states and $5d$ conduction-band states and from electric-quadrupole transitions coupling $2p$ core states and $4f$ states (consistent with Table I). For simplicity, we also assume that the degree of linear polarization of the incident beam $P=1$. Then, the amplitude for the π-polarized component of the magnetic scattering is

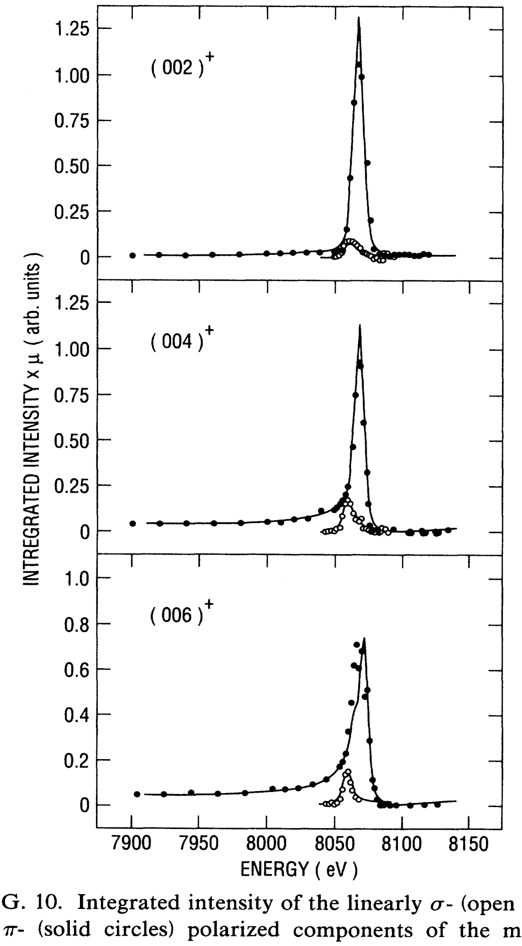

FIG. 10. Integrated intensity of the linearly σ- (open circles) and π- (solid circles) polarized components of the magnetic scattering plotted as the incident x-ray energy is tuned through the $L_{\rm III}$ absorption edge for the $(0,0,2+\tau)$, $(0,0,4+\tau)$, and $(0,0,6+\tau)$ reflections. Solid lines are the results of fits, which are discussed in the text.

$$|f_{\sigma\text{-}\pi}|^2=\mathcal{A}_1\left|J_{\text{eff}}\frac{\hbar\omega}{mc^2}\sin(2\theta)\sin(\theta)+\frac{\cos(\theta)}{\Gamma(x-i)}\left[A-\frac{B}{\Gamma(x-i)}\right]+\frac{\cos(\theta)\cos(2\theta)C}{\Gamma(x'-i)}\right|^2 , \tag{7}$$

where

$$J_{\text{eff}}=(\tfrac{3}{5}f_L+\tfrac{1}{5}f_S)J=\begin{cases}5.5 & \text{for } (0,0,2+\tau),\\ 4.0 & \text{for } (0,0,4+\tau),\\ 2.3 & \text{for } (0,0,6+\tau)\ ,\end{cases}$$

$$A=\frac{Fn_e}{4}\ ,$$

$$B=\frac{n_hF\Delta}{4}\ ,$$

and

$$C=F'\ .$$

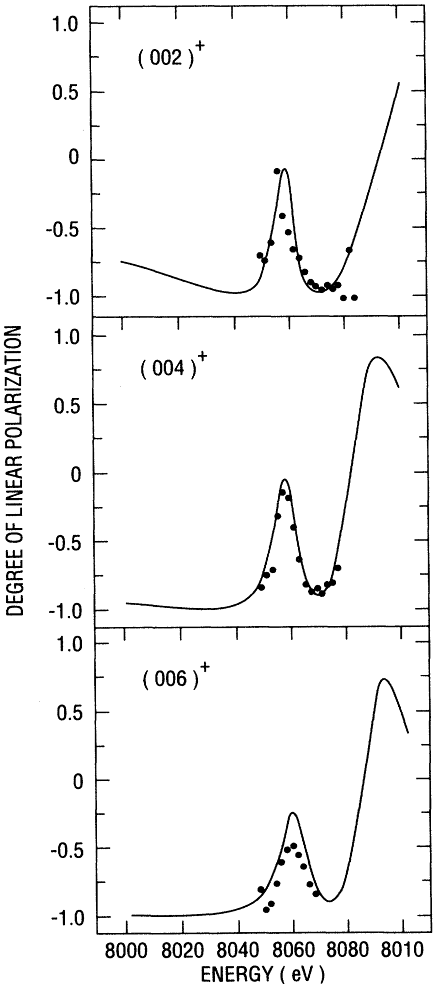

FIG. 11. The degree of linear polarization for the $(0,0,2+\tau)$, $(0,0,4+\tau)$, and $(0,0,6+\tau)$ magnetic reflections, plotted as the incident x-ray energy is tuned through the L_{III} absorption edge. The solid lines are the degree of linear polarization calculated from the fits shown in Figs. 9 and 10.

In this expression, the term containing J_{eff} is the π-polarized component of the nonresonant contribution to the magnetic scattering for a magnetic spiral[14] and depends on the form factors for the orbital- and spin-magnetization densities f_L and f_S. The values for J_{eff} listed in Eq. (7) are calculated from published values[43] and are consistent with the results of Sec. V. The terms containing A and B are the resonant contributions from electric-dipole transitions coupling $2p$ and spin-down and spin-up $5d$ orbitals. n_e and n_h are, respectively, the net induced polarization and the number of holes in the $5d$ band of holmium, and Δ is the energy of the exchange splitting between spin-down and spin-up states in the d band. F represents the contribution from the F_{LM}'s in Eq. (6) and depends on the overlap of radial $2p$ and $5d$ electronic wave functions. The principal effect of the exchange splitting in Eq. (7) is to introduce a second-order pole with amplitude proportional to B. Γ is the width of the excited resonant state, and $x=2(E_a-E_b-\hbar\omega)/\Gamma$ is the resonant denominator. The term containing C is the resonant contribution from electric quadrupole transitions coupling $2p$ and $4f$ states. The 6-eV shift which appears in the resonant denominator of the quadrupole term

$$x'=2(E_a-E_b-\hbar\omega-6)/\Gamma$$

accounts for the 6-eV splitting which separates the dipole and quadrupole excitations evident in the data (see Fig. 8). The trigonometric functions in Eq. (7) give the polarization dependence of the resonant and nonresonant cross sections for a magnetic spiral, and depend on the scattering angle. $\mathcal{A}_1$ is a global scale factor, independent of scattering angle 2θ, which accounts for the structure factor, the Debye-Waller factor, the incident intensity, etc.

The amplitude for the σ-polarized component of the magnetic scattering is similarly written:

$$|f_{\sigma\text{-}\sigma}|^2=\mathcal{A}_1\left|\frac{\hbar\omega}{mc^2}S_{\text{eff}}\sin(2\theta)-\frac{C'\sin(2\theta)}{\Gamma(x'-i)}\right|^2 , \tag{8}$$

where

$$S_{\text{eff}}=\tfrac{1}{5}f_SJ=\begin{cases}1.4 & \text{for } (0,0,2+\tau),\\ 0.9 & \text{for } (0,0,4+\tau),\\ 0.6 & \text{for } (0,0,6+\tau)\ .\end{cases}$$

For the σ-polarized component and $P=1$, only the spin-magnetization density contributes to the nonresonant magnetic scattering. Because the contributions to the amplitude for the magnetic scattering from $f_{\sigma\text{-}\sigma}$ are small, we neglect them in the model for the total cross section (that is, for the data in Fig. 11), and simply use Eq. (7) with a new scale factor $\mathcal{A}_2$. From the measured efficiency of the polarization analyzer with PG (0,0,6) at $\hbar\omega=8100$ eV, $\mathcal{A}_2$ is constrained to equal $\sim 16\mathcal{A}_1$. The adjustable parameters in the model of Eqs. (7) and (8) are, therefore, $\mathcal{A}_1$, A, B, C, C', and Γ.

Self-consistent fits of the data to the model are shown by the solid lines in Figs. 9–11. Because these parameters are highly correlated, it has not been possible to obtain "best fits" of the results, which would result from arbitrary variations of the parameters. Instead, these values have emerged after repeated trials starting from a variety of initial values. Small variations of the parameters may also give reasonable fits.[47] Although the results are approximate, certain features of the resulting line shapes are clear and suggest that the basic elements of the description are correct. In particular, it is seen that the asymmetric tail and the large enhancement near the $L_{\rm III}$ absorption edge for the total cross section in Fig. 9 and for the π-polarized component of Fig. 10 are closely reproduced. On the basis of the model, it is unambiguous that this asymmetry arises from the interference of the resonant and nonresonant cross sections in Eq. (7). It may also be deduced that the decreased asymmetry in the line shape for the $(0,0,2+\tau)$ reflection results from the decrease of the nonresonant magnetic cross-section scattering [due to $\sin(\theta)$ in Eq. (4)] at small momentum transfers.

A second result of the fitting concerns the apparent broadening or fine structure of the line shapes of the $(0,0,6+\tau)$ reflections, relative to the line shapes of the $(0,0,4+\tau)$ and $(0,0,2+\tau)$ reflections, in both Figs. 9 and 10. Although the agreement is not precise, it seems clear from the model that the weak shoulder which becomes visible at higher momentum transfers arises from quadrupole contributions to the π-polarized component of the magnetic scattering [that is, from the term containing C in Eq. (7)]. This manifestation of the quadrupole contributions at higher momentum transfers is a consequence of the polarization dependence of the resonant cross section. It is also noteworthy that Eq. (8) provides a reasonable description of the σ-polarized components of the magnetic scattering, both with regard to their intensity relative to the π-polarized components (which was used to fix the value of C') and with regard to the possibility of a weak line shape asymmetry toward higher energies.

The values of the parameters used to generate the fits shown in Figs. 9–11 are $\mathcal{A}_1=0.03$, $A=2$, $B=4$, $-C=C'=\frac{3}{4}$, and $\Gamma=9$ eV. The fitted level with $\Gamma=9$ eV is close to the atomic value calculated for holmium of about 7 eV.[48] It is interesting that the ratio of the fitted constants $A/B=\frac{1}{2}$ is of the same order of magnitude as may be estimated from reasonable values of the parameters for holmium: $A/B=n_e/n_h\Delta=\frac{1}{8}$ with $n_h\sim 8$, $n_e\sim 0.2$, and $\Delta=0.2$ eV. Similarly, the fitted values of the constants A and B each fall within a factor of 2 of the values obtained using one-electron orbitals in a calculation of the F_{LM}'s for $({\rm Ho})^3$. Using the same estimates for n_h, n_e, and Δ as above, these calculations[2,3] yield $A\sim 1$ and $B\sim 8$. Thus, the fitted parameters A and B are qualitatively consistent with one-electron predictions for the electronic structure. The discrepancies between the fitted parameters and their calculated values suggest that more sophisticated calculations of the electronic structure may be required before a quantitative comparison is possible. In the calculation, for example, the influence of the core hole on the wave functions of the excited state has been ignored. It should be clearly noted, in addition, that the effect of the exchange splitting on the model may be entirely removed by setting $B=0$ in Eq. (7) above. Fits of the model with $B=0$ have also been successfully performed, leading to results of nearly the same quality as those shown in Figs. 9 and 10. For this range of the parameters, the main effect of the exchange splitting on the line shapes is to introduce small corrections to the maximum intensity. Therefore, while the present results are consistent with an orbital model of the electronic structure which includes exchange splitting of the d band, these fits are not unique. Finally, we note the values of the constant C and C' are of the same order of magnitude as A and B, but that C has opposite sign to the results expected from one-electron calculations. It seems possible that this difference may reflect the influence of the crystal field, which has also been ignored in the calculation.[2,3]

Before concluding this discussion, we illustrate certain features of the resonant line shapes in more detail. The solid line in Fig. 12 shows the fit of the $(0,0,4+\tau)$ reflection in Fig. 10, plotted on a logarithmic scale from $\hbar\omega=7600$ to 8600 eV. Plotted on this scale, there is a clear interference minimum just above the resonant maximum. Although the decrease of the magnetic scattering measured above the $L_{\rm III}$ edge in holmium is abrupt, the observed scattering is still too weak to permit observation of the minimum. The dashed line in Fig. 12 shows the energy dependence of the nonresonant scattering for the $(0,0,4+\tau)$, obtained from Eq. (7) by setting $A=B=C=0$. As expected, the resonant cross section approaches the nonresonant cross section at x-ray ener-

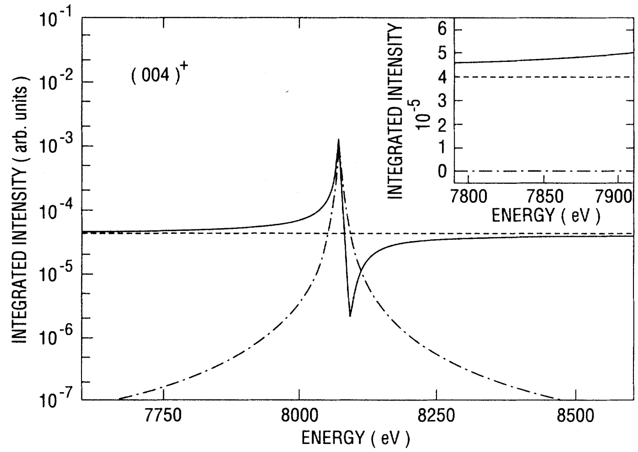

FIG. 12. Solid line: fit of the energy dependence of the magnetic scattering at the $(0,0,4+\tau)$ reflection, including resonant and nonresonant contributions, and plotted on a logarithmic scale. Dashed line: Energy dependence of the nonresonant magnetic scattering [obtained from the fit of the $(0,0,4+\tau)$ line shape by setting $A=B=C=0$ in Eq. (7)]. Dash-dotted line: Energy dependence of the resonant magnetic scattering [obtained from the fit of the $(0,0,4+\tau)$ line shape by setting $J_{\rm eff}=0$ in Eq. (7)]. Inset: Same as above, but plotted on a linear scale between $\hbar\omega=7800$ and 7900 eV, near where the off-resonant experiments were performed.

gies sufficiently far from the $L_{\rm III}$ edge. These same line shapes are shown in the inset in Fig. 12, plotted on a linear scale between $\hbar\omega = 7800$ and 7900 eV. This is, the range of energy in which the off-resonance experiments described in Sec. V were performed. From the inset it is clear that the resonant contributions to the π-polarized component are of the order of 20% of the nonresonant contributions. Similar statements hold for the $(0,0,2+\tau)$ and $(0,0,6+\tau)$ magnetic reflections, and for all of the σ-polarized components. It is on the basis of these calculations that estimates of the magnitude of the resonant contributions were made in the discussion of Fig. 4. The dashed line in Fig. 12 shows the energy dependence of the pure resonant scattering, obtained from Eq. (7) by setting $J_{\rm eff} = 0$. In the absence of a nonresonant contribution, the line-shape asymmetry characteristic of the data is completely lost. In fact, as may be seen by the dashed line inset in the figure, pure resonant magnetic scattering is unobservable on a linear scale below about $\hbar\omega = 8000$ eV. Finally, we note that estimates of the magnitude of the corrections to the resonant cross section near the $L_{\rm III}$ absorption edge from the $M_{\rm IV}$ and $L_{\rm II}$ edges were made and found to be negligibly small.

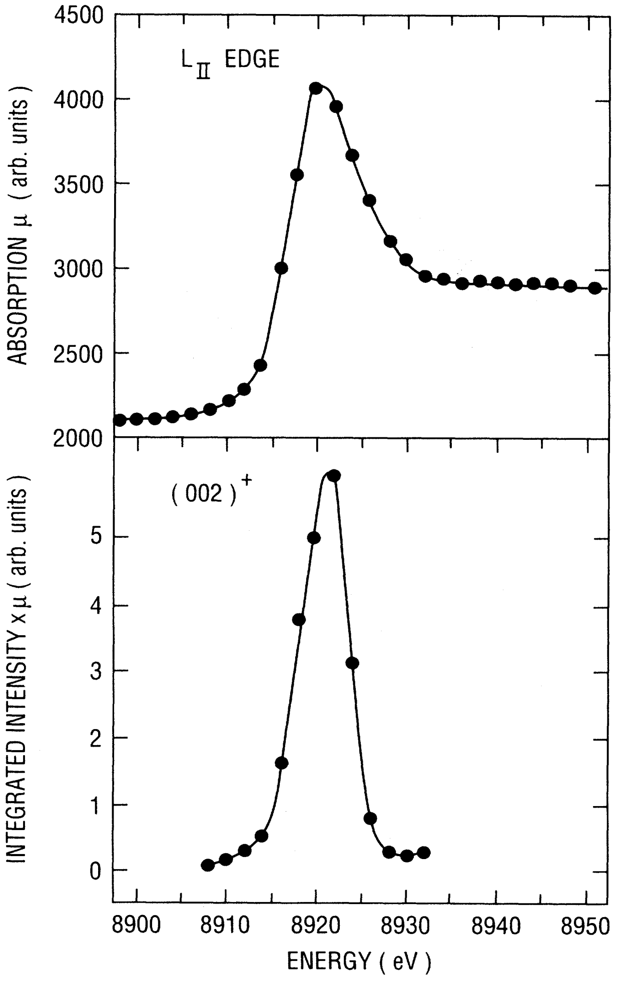

FIG. 13. Top: The absorption measured through a 5 μm holmium film as the incident x-ray energy is tuned through the $L_{\rm II}$ edge. Bottom: Integrated magnetic intensity of the $(0,0,2+\tau)$ reflection plotted vs incident x-ray energy. The solid lines are drawn only to guide the eye.

C. $L_{\rm II}$ and $L_{\rm I}$ absorption edges

The energy dependence of the integrated magnetic intensity obtained from the $(0,0,2+\tau)$ reflection of holmium is plotted for incident x-ray energies near the $L_{\rm II}$ edge at $\hbar\omega = 8916$ eV in the lower panel of Fig. 13. The data have been corrected for the absorption, which is shown plotted in the top panel. Similar to the results obtained for energies near the $L_{\rm III}$ absorption edge, a resonant increase in the magnetic scattering near the $L_{\rm II}$ absorption edge is observed with an energy FWHM of about 10 eV. Compared to the maximum intensity measured at the $L_{\rm III}$ edge, the maximum intensity measured at the $L_{\rm II}$ edge is reduced by about a factor of 10. Assuming that the magnetic scattering is dominated by electric-dipole transitions coupling $2p_{1/2}$ and $5d_{3/2}$ atomic orbitals, one-electron calculations of the F_{LM}'s in Eq. (6) suggest that the enhancement obtained at the $L_{\rm II}$ edge should be of the same order of magnitude as that obtained at the $L_{\rm III}$ edge. We were unable to detect resonant second harmonics at the $L_{\rm II}$ absorption edge, and did not perform polarization analysis of the magnetic scattering at τ.

The energy dependence of the magnetic scattering ob-

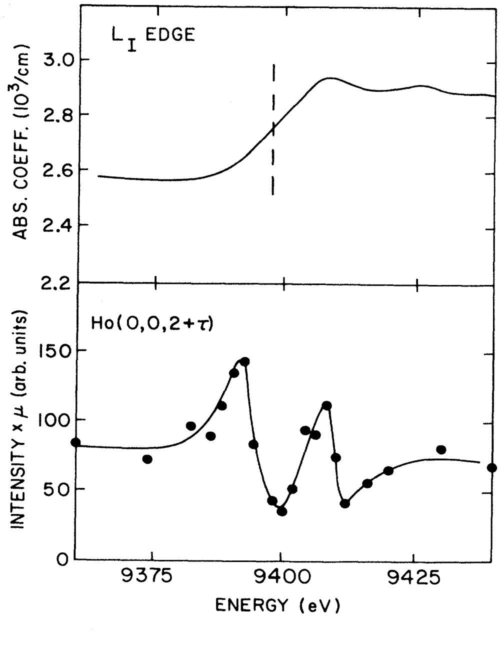

FIG. 14. Top: The absorption measured through a 5 μm holmium film as the incident x-ray energy is tuned through the $L_{\rm I}$ edge. Bottom: integrated magnetic intensity of the $(0,0,2+\tau)$ reflection plotted vs incident x-ray energy. The solid lines are drawn only to guide the eye.

tained from the $(0,0,2+\tau)$ magnetic reflection for incident x-ray energies near the $L_{\rm I}$ absorption edge at $\hbar\omega=9395$ eV is shown in the lower panel of Fig. 14. The data have been corrected for the absorption, which is shown in the top panel. In this case, the absorption is dominated by electric-dipole transitions coupling 2*s* core states and 6*p*-derived conduction-band states. The scattering measured at τ near the $L_{\rm I}$ edge is rather weak, which makes reliable integrated intensities difficult to obtain. While their existence cannot be regarded as definitively established by the data, nevertheless, the solid line drawn through the data points in Fig. 14 suggests the possibility that the magnetic scattering exhibits two peaks, split in energy by about 15 eV. Similar behavior has been observed in spin-dependent absorption measurements on holmium compounds near the $L_{\rm I}$ edge by Schütz and co-workers.[49] Because the overlap of the 2*s* and 6*p* atomic wave functions in holmium is small, resonant electric-dipole contributions to the magnetic scattering are also expected to be small. Calculations of the electric quadrupole $(2s\rightarrow5d)$ and octupole $(2s\rightarrow4f)$ transitions suggest that these terms may be as large as the dipole term at the $L_{\rm I}$ edge[2,3] and may contribute to the splitting shown in Fig. 14.

D. High-Q-resolution experiments

To investigate the energy dependence of the scattering profiles with high Q resolution, a Ge(111) analyzing crystal was placed on the 2θ arm before the detector, and radial and transverse scans of the $(0,0,2+\tau)$ magnetic satellite were made as the incident energy was tuned through the $L_{\rm III}$ absorption edge. In these experiments the scattering angle of the analyzing crystal was incremented and the magnetic signal was optimized at each energy. Representative scans of the radial profiles for the

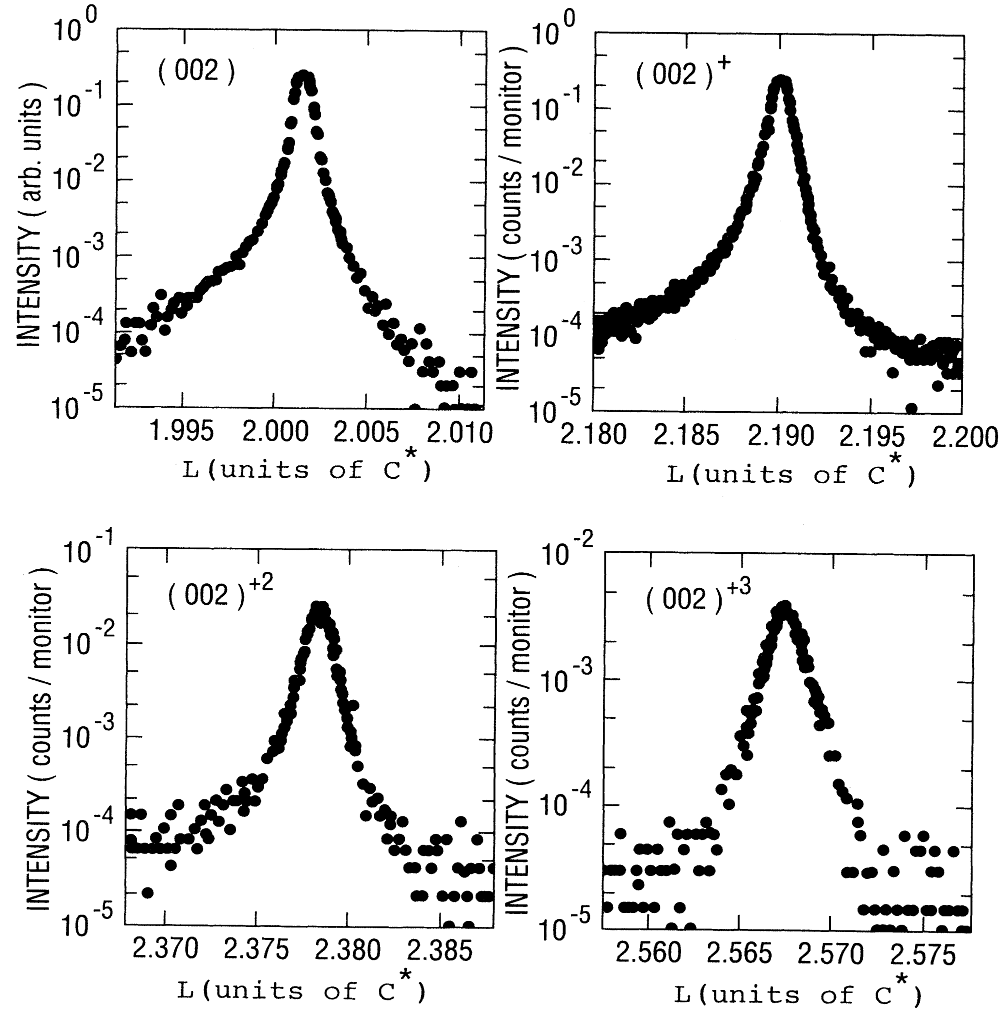

FIG. 15. High-Q-resolution scans taken along the $[0,0,L]$ direction and plotted on a logarithmic scale of the charge scattering at the (0,0,2) reflection, and of the magnetic scattering at the $(0,0,2+\tau)$, $(0,0,2+2\tau)$, and $(0,0,2+3\tau)$ reflections. These data were taken with the incident x-ray energy $\hbar\omega=8062$ eV, where the contributions from quadrupole transitions are a maximum.

$(0,0,2)$, $(0,0,2+\tau)$, $(0,0,2+2\tau)$, and $(0,0,2+3\tau)$ reflections at $T=35$ K are shown in Fig. 15, plotted on a logarithmic scale. These scans were taken at an energy $\hbar\omega=8062$ eV, at which energy the contributions from electric-quadrupole transitions are a maximum. The FWHM of these peaks along the $[0,0,L]$ direction for the $(0,0,2)$, $(0,0,2+\tau)$, $(0,0,2+2\tau)$, and $(0,0,2+3\tau)$ reflections are, respectively, $\Delta l=0.0008c^*$, $0.0009c^*$, $0.0012c^*$, and $0.0016c^*$. These widths correspond to structural and magnetic correlation lengths of several thousand Å, or greater. The broadening of the radial profiles with increasing momentum transfer reflects, in part, the Q dependence of the resolution function. Despite the broadening, it seems clear from Fig. 15 that the line shapes of the resonant charge and magnetic scattering are all closely similar, and, further, that the line shapes for the $(0,0,2)$ and $(0,0,2+\tau)$ reflections are identical.

The FWHM of the radial and transverse profiles (determined from Gaussian and Lorentzian fits below and above the edge, respectively) for the $(0,0,2+\tau)$ magnetic satellite are plotted versus incident x-ray energy in Fig. 16. In both cases the widths are approximately constant below the inflection point of the L_{III} absorption edge (indicated by the dashed line in the figure), but increase by 20% near the edge. Above the edge, the radial and transverse widths are reduced from their maximum values, but remain larger than their original values. This behavior is strikingly similar to the absorption, and suggests that the broadening is related to the increased absorption at the L_{III} edge. It is noteworthy in this regard that the absorption length of holmium at these energies and the correlation length are each of the same order of magnitude—about 1 μm. In contrast, the extinction length for magnetic scattering (assuming a hundredfold resonant enhancement) is about ten times longer. It therefore seems reasonable to suppose that the observed broadening originates in the decreased penetration depth, relative to the correlation length, at the L_{III} edge. This result illustrates the surface, and near-surface, sensitivity of x-ray magnetic scattering. It is also worth noting that the energy dependence of the integrated intensity obtained from the high-resolution scans discussed here closely matches the results shown in Figs. 9 and 10.

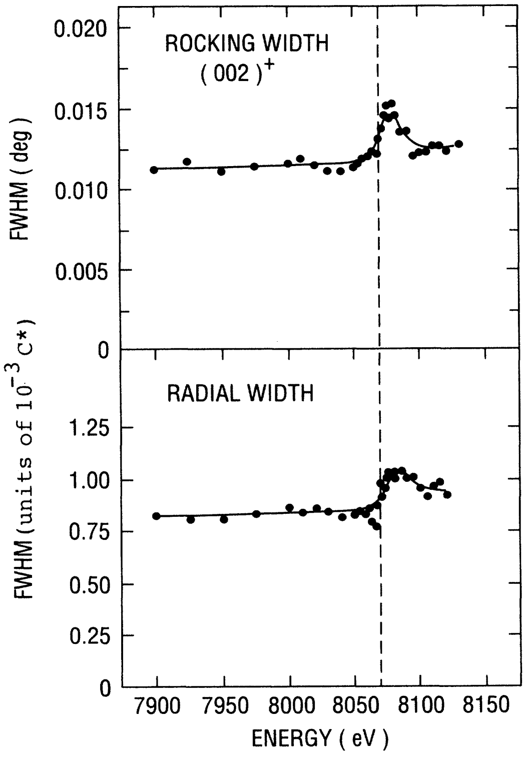

FIG. 16. Rocking and radial widths of the $(0,0,2+\tau)$ magnetic satellite plotted as the incident x-ray energy is tuned through the L_{III} absorption edge.

E. Temperature dependence

We have investigated the temperature dependence of the magnetic scattering from $T=32$ K up to and above the Néel temperature near $T=138$ K, for incident x-ray energies both near to the L_{III} absorption edge and about 200 eV below it. The square root of the integrated intensity of the $(0,0,2+\tau)$ magnetic satellite, obtained in a low-resolution configuration, is plotted on a logarithmic scale versus temperature. in Fig. 17. The off-resonant cross section was obtained at $\hbar\omega=7900$ eV and the resonant cross section was obtained at $\hbar\omega=8067$ eV, the energy at which the contributions from electric-dipole transitions are maximum. In both cases, the order parameter approaches zero near $T=138$ K in a manner characteristic of a continuous phase transformation. To within the

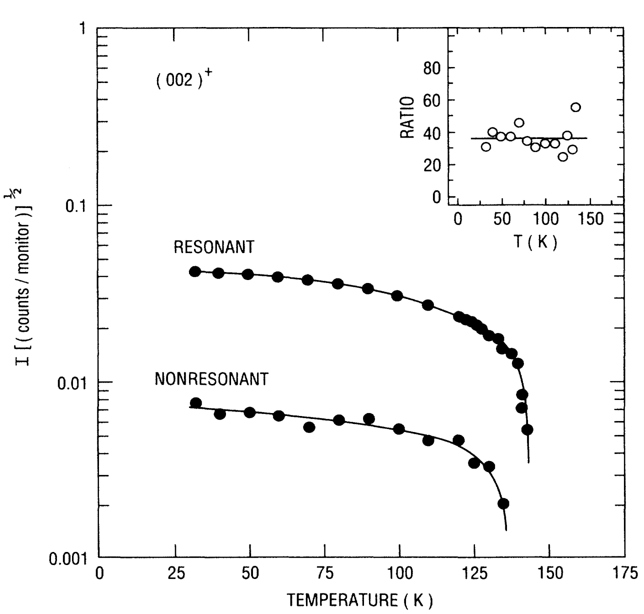

FIG. 17. Temperature dependence of $I^{1/2}$ for the resonant and off-resonant cross sections. The Néel temperature of holmium is about $T=138$ K. Inset: Temperature dependence of the ratio of the resonant and off-resonant cross sections. Solid lines are drawn only to guide the eye.

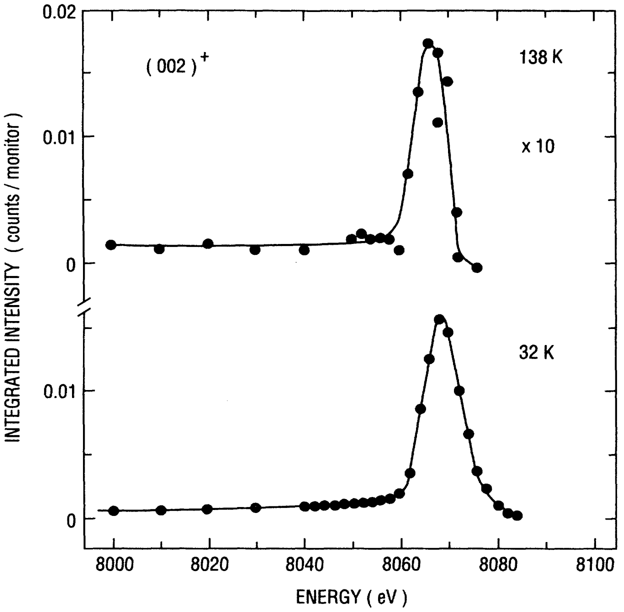

FIG. 18. Energy dependence of the magnetic scattering for the $(0,0,2+\tau)$ reflection obtained just below the Néel point at $T=138$ and 32 K. Solid lines are drawn only to guide the eye.

counting statistics obtained for the nonresonant cross section, the ratio of the resonant intensity to that of the nonresonant intensity is a constant equal to about 40 (see inset). With the sample temperature fixed at $T=138$ K, we have also studied the energy dependence of the magnetic scattering of the $(0,0,2+\tau)$ magnetic satellite. As shown in Fig. 18, the line shape of the magnetic scattering versus incident x-ray energy obtained at $T=138$ K is identical to that obtained at $T=32$ K, to within counting statistics. It is interesting that preliminary investigations of the temperature dependence of the higher harmonics suggest that the integrated intensity for 3τ may fall off faster than that for τ or 2τ above 90 K. Finally, for temperatures increasing through the Néel temperature in steps of about 1 K, no critical magnetic scattering was observed in holmium either near to or far from resonance.

VII. CONCLUSIONS

We have presented a study of the polarization and resonance properties of the x-ray magnetic cross section of the spiral antiferromagnet holmium for incident x-ray energies near to and far from the L_{III}, L_{II}, and L_{I} absorption edges. Off resonance, that is, 200 eV below the L_{III} edge, we have measured the degree of linear polarization of the x-ray cross section for several different chemical and magnetic reflections and shown that the dependence of the degree of linear polarization on momentum transfer is consistent with a simple nonresonant description. This suggests, in particular, that the results for the magnetic scattering are mainly determined by the large orbital magnetic moment in holmium. We have also observed resonant enhancements of the magnetic scattering at each of the L_{I}, L_{II}, and L_{III} absorption edges. Near the L_{III} edge, we have made systematic measurements of the line shapes of the total magnetic scattering, of the linear σ- and π-polarized components of the magnetic scattering, and of their resonant harmonics. These results are qualitatively consistent with the theory of x-ray resonance exchange scattering, including electric-dipole and -quadrupole transitions among atomic orbitals. The most striking feature of the line shapes is their asymmetry, which arises from the interference of the resonant and nonresonant contributions. It remains to explain the quantitative deviations of the fitted parameters for the L_{III} resonance behavior from simple one-electron estimates and to explain the weakness of the enhancement observed near the L_{II} absorption edge relative to that observed near the L_{III} edge. In our view, x-ray magnetic scattering techniques will find continued fruitful application in studies of rare earths, actinides, transition elements, and their compounds—particularly in the extensions of these studies to thin films, multilayers, and surface layers. It also seems clear that these techniques will benefit directly from the development of polarization- and energy-tunable insertion-device beamlines at the high-brightness storage rings under construction in the United States, Europe, and Japan.

ACKNOWLEDGMENTS

We have benefitted from discussions with J. D. Axe, J. Bohr, M. Blume, J. P. Hannon, J. B. Hastings, D. P. Siddons, S. K. Sinha, and G. T. Trammell. The work performed at Brookhaven National Laboratory is supported by the U. S. Department of Energy under Contract No. DE-AC02-76CH00016. CHESS is supported by the National Science Foundation under Grant No. DMR-84112465.

---

[*] Present address: National Synchrotron Light Source, Brookhaven National Laboratory, Upton, NY 11973.

[†] Present address: Argonne National Laboratory, 9700 South Cass Avenue, Argonne, Illinois 60439.

[‡] Present address: European Synchrotron Radiation Facility, 38043 Grenoble Cedex, France.

[1] D. Gibbs, D. R. Harshman, E. D. Isaacs, D. B. McWhan, D. Mills, and C. Vettier, Phys. Rev. Lett. **61**, 1241 (1988).

[2] J. P. Hannon, G. T. Trammell, M. Blume, and D. Gibbs, Phys. Rev. Lett. **61**, 1245 (1988).

[3] J. P. Hannon, G. T. Trammell, M. Hamrick, and M. Blume (unpublished).

[4] W. C. Koehler, J. W. Cable, M. K. Wilkinson, and E. O. Wollan, Phys. Rev. **151**, 414 (1966).

[5] W. C. Koehler, J. W. Cable, H. R. Child, M. K. Wilkinson, and E. O. Wollan, Phys. Rev. **158**, 450 (1967).

[6] D. T. Keating, Phys. Rev. **178**, 732 (1969).

[7] G. P. Felcher, G. H. Lander, T. Arai, S. K. Sinha, and F. H. Spedding, Phys. Rev. B **13**, 3034 (1976).

[8] M. Pechan and C. Stassis, J. Appl. Phys. **55**, 1900 (1984).

[9] D. Gibbs, D. E. Moncton, K. L. D'Amico, J. Bohr, and B. Grier, Phys. Rev. Lett. **55**, 234 (1985).

[10] J. Bohr, D. Gibbs, D. E. Moncton, and K. L. D'Amico, Physica A **140**, 349 (1986).

[11] J. Bohr, D. Gibbs, J. D. Axe, D. E. Moncton, K. L. D'Amico, C. F. Majkrzak, J. Kwo, M. Hong, C. L. Chien, and J. Jensen, Physica B **159**, 93 (1989).

[12] R. A. Cowley and S. Bates, J. Phys. C **21**, 4113 (1988).

[13] M. Blume, J. Appl. Phys. **57**, 3615 (1985).

[14] M. Blume and D. Gibbs, Phys. Rev. B **37**, 1779 (1988).

[15] S. W. Lovesey, J. Phys. C **20**, 5625 (1987).

[16] E. D. Isaacs, D. B. McWhan, C. Peters, G. E. Ice, D. P. Siddons, J. B. Hastings, C. Vettier, and O. Vogt, Phys. Rev. Lett. **62**, 1671 (1989).

[17] D. B. McWhan, C. Vettier, E. D. Isaacs, G. E. Ice, D. P. Siddons, J. B. Hastings, C. Peters, and O. Vogt, Phys. Rev. B **42**, 6007 (1990).

[18] W. Kaiser, Ph.D thesis, University of München, 1989.

[19] E. D. Isaacs, D. B. McWhan, D. P. Siddons, J. B. Hastings, and D. Gibbs, Phys. Rev. B **40**, 9336 (1989).

[20] J. Bohr, D. Gibbs, and K. G. Huang, Phys. Rev. B **42**, 4322 (1990).

[21] D. Gibbs, J. Bohr, J. D. Axe, D. E. Moncton, and K. L. D'Amico, Phys. Rev. B **34**, 8182 (1986); M. Sanyal, D. Gibbs, J. Bohr, and M. Wulf (unpublished).

[22] C. Vettier, D. B. McWhan, E. M. Gyorgy, J. Kwo, B. M. Buntschuh, and B. W. Batterman, Phys. Rev. Lett. **56**, 757 (1986).

[23] C. F. Majkrzak, D. Gibbs, J. Bohr, and J. Kwo (unpublished).

[24] W. G. Stirling, W. Buyers, E. D. Isaacs, D. B. McWhan, C. Peters, G. E. Ice, D. P. Siddons, and J. B. Hastings (unpublished).

[25] E. D. Isaacs, D. B. McWhan, R. F. Kleiman, P. Zschock, G. E. Ice, B. Gaulin, T. Mason, J. D. Garrett, and W. L. J. Buyers, Phys. Rev. Lett. **65**, 3185 (1990).

[26] W. G. Stirling, D. Jones, G. H. Lander, W. Herzog, C. C. Tang, D. Gibbs, and P. Cama (unpublished).

[27] K. Namikawa, M. Ando, T. Nakajima, and H. Kawata, J. Phys. Soc. Jpn. **54**, 4099 (1985).

[28] A. Goldman, K. M. Mohanty, G. Shirane, T. R. Thurston, C. J. Peters, R. J. Birgeneau, R. L. Greene, and P. M. Horn, Phys. Rev. B **36**, 5609 (1987); T. R. Thurston, C. J. Peters, R. J. Birgeneau, and P. M. Horn, *ibid.* **37**, 9559 (1988).

[29] C. Kao, J. B. Hastings, E. D. Johnson, D. P. Siddons, G. C. Smith, and G. A. Prinz, Phys. Rev. Lett. **65**, 373 (1990).

[30] G. Schütz, M. Knulle, R. Wienke, W. Wilhelm, W. Wagner, P. Kienle, and R. Frahm, Z. Phys. B **73**, 67 (1988).

[31] P. Carra, M. Altarelli, and F. deBergevin, Phys. Rev. B **40**, 7324 (1989); P. Carra and M. Altarelli, Phys. Rev. Lett. **64**, 1284 (1990).

[32] F. deBergevin and M. Brunel, Phys. Lett. **39A**, 141 (1972).

[33] F. deBergevin and M. Brunel, Acta Crystallogr. A **37**, 314; 324 (1981).

[34] P. Platzman and N. Tsoar, Phys. Rev. B **2**, 3556 (1972).

[35] M. Brunel, G. Patraff, F. deBergevin, F. Rousseau, and M. Lemonnier, Acta Crystallogr. A **39**, 83 (1984).

[36] A. J. Bevalo, B. J. Beaudry, and K. A. Gschneidner, J. Electrochem. Soc. **127**, 2556 (1980).

[37] D. Gibbs, M. Blume, D. R. Harshman, and D. B. McWhan, Rev. Sci. Instrum. **60**, 1655 (1989).

[38] *Handbook on the Physics and Chemistry of Rare Earth Metals*, edited by K. A. Gschneidner and L. Eyring (North-Holland, Amsterdam, 1978), Vol. 1.

[39] J. K. Lang, Y. Bauer, and P. A. Cox, J. Phys. F **11**, 121 (1981).

[40] J. O. Dimmock and A. J. Freeman, Phys. Rev. Lett. **13**, 750 (1964); J. F. Herbst, D. N. Lowy, and R. E. Watson, Phys. Rev. B **6**, 1913 (1972).

[41] R. A. Cowley, Adv. Phys. **29**, 1 (1980).

[42] It is worth noting that the degree of linear polarization P_m' for any magnetic structure obtained from a simple spiral structure by the introduction of a layer-dependent phase factor will also be described by Eq. (4). Thus, while both the bunching of the moments in holmium due to the crystal field and the presence of spin slips (Refs. 9–11) may alter the absolute magnetic intensity, and introduce additional satellites, these distortions will leave the degree of linear polarization unaffected. Contributions to the magnetic scattering at τ from the ferromagnetic component of the conical structure are negligible. Finally, we remark that, although the possibility that additional charge scattering may exist along the c axis at τ cannot be entirely ruled out, its existence is not consistent with the present results.

[43] M. Blume, A. J. Freeman, and R. E. Watson, J. Chem. Phys. **37**, 1242 (1962); **41**, 1878 (1964).

[44] The scatter apparent in the data for 3τ and 4τ above $\hbar\omega = 8070$ eV in Fig. 7 is enhanced by the absorption correction, which is large at these energies. Little or no scattered intensity was actually observed above the background at 3τ and 4τ for $\hbar\omega > = 8070$ eV.

[45] The 6-eV splitting between dipole and quadrupole contributions was determined at CHESS where the energy resolution was about 2 eV. In this paper, no particular significance is attached to the "inflection point of the absorption," except as a reference for the incident photon energy.

[46] The maximum intensity measured for the $(0,0,4+\tau)$ reflection before correction by the Lorentz factor is reduced from the intensity for the $(0,0,2+\tau)$ reflection by about a factor 2.

[47] After the data for the $(0,0,6+\tau)$ reflection had been collected, it was discovered that the measured intensities of the π-polarized component were inconsistent by a factor of 1.6 with the results obtained for the total cross section at the $(0,0,6+\tau)$ and with the results for the nonresonant cross section. For this reason an additional scale factor of 1.6 has been introduced in the fits of the π-polarized component of the $(0,0,6+\tau)$ reflection.

[48] M. H. Chen, B. Crasemann, and H. Mark, Phys. Rev. A **21**, 449 (1980).

[49] G. Schütz (private communication).